Redshift-space equal-time angular-averaged consistency relations of the gravitational dynamics

Takahiro Nishimichi, Patrick Valageas

PHYSICAL REVIEW D **92,** 123510 (2015)

Redshift-space equal-time angular-averaged consistency relations of the gravitational dynamics

Takahiro Nishimichi[1,2,3,4] and Patrick Valageas[5]

[1]*Sorbonne Universités, UPMC Univ Paris 06 UMR 7095, Institut d'Astrophysique de Paris, F-75014 Paris, France*

[2]*CNRS, UMR 7095, Institut d'Astrophysique de Paris, F-75014 Paris, France*

[3]*Kavli Institute for the Physics and Mathematics of the Universe, The University of Tokyo Institutes for Advanced Study, 5-1-5 Kashiwanoha, Kashiwa 277-8583, Japan*

[4]*CREST, JST, 4-1-8 Honcho, Kawaguchi, Saitama 332-0012, Japan*

[5]*Institut de Physique Théorique, Université Paris Saclay, CEA, CNRS, F-91191 Gif-sur-Yvette, France*

(Received 18 August 2015; published 9 December 2015)

We present the redshift-space generalization of the equal-time angular-averaged consistency relations between $(\ell + n)$- and n-point polyspectra (i.e., the Fourier counterparts of correlation functions) of the cosmological matter density field. Focusing on the case of the $\ell = 1$ large-scale mode and n small-scale modes, we use an approximate symmetry of the gravitational dynamics to derive explicit expressions that hold beyond the perturbative regime, including both the large-scale Kaiser effect and the small-scale fingers-of-god effects. We explicitly check these relations, both perturbatively, for the lowest-order version that applies to the bispectrum, and nonperturbatively, for all orders but for the one-dimensional dynamics. Using a large ensemble of N-body simulations, we find that our relation on the bispectrum in the squeezed limit (i.e., the limit where one wave number is much smaller than the other two) is valid to better than 20% up to 1 $h\mathrm{Mpc}^{-1}$, for both the monopole and quadrupole at $z = 0.35$, in a ΛCDM cosmology. Additional simulations done for the Einstein–de Sitter background suggest that these discrepancies mainly come from the breakdown of the approximate symmetry of the gravitational dynamics. For practical applications, we introduce a simple *ansatz* to estimate the new derivative terms in the relation using only observables. Although the relation holds worse after using this *ansatz*, we can still recover it within 20% up to 1 $h\mathrm{Mpc}^{-1}$, at $z = 0.35$ for the monopole. On larger scales, $k = 0.2$ $h\mathrm{Mpc}^{-1}$, it still holds within the statistical accuracy of idealized simulations of volume ~ 8 $h^{-3}\mathrm{Gpc}^3$ without shot-noise error.

DOI: 10.1103/PhysRevD.92.123510 PACS numbers: 98.80.-k

I. INTRODUCTION

An accurate understanding of the nonlinear gravitational dynamics is a key for observational projects that measure the statistical properties of the cosmic structures on large scales. The typical scales of interest in these projects range from the weakly to the strongly nonlinear regimes [1,2]. While perturbation theory is expected to be applicable as long as the nonlinear corrections are subdominant [3,4], a fully nonlinear description would be helpful to extract cosmological information out of the measured statistics over a wider dynamic range. The analytical description also becomes more complicated when one models higher-order statistics. Although an increasing number of analytical techniques to calculate the power spectrum or the two-point correlation function have been proposed, based for instance on resummations of perturbative series expansion or effective approaches [5–16], few of them have been applied to the bispectrum or even higher orders.

Consistency relations n-point correlation functions (or polyspectra in Fourier space) are then very useful to have an accurate description of the higher-order statistics once one has a reliable model for the lowest-order one, the power spectrum. Alternatively, they can be used to test analytical models, numerical simulations, or the underlying cosmological scenario (e.g., the impact of modified gravity or complex dark energy models). Based on the assumption of Gaussian initial conditions and gravitational dynamics governed by general relativity, these relations hold at the nonperturbative level and provide a rare insight into the nonlinear regime of gravitational clustering.

The most generic consistency relations are "kinematic consistency relations" that relate the $(\ell + n)$-density correlation, with ℓ large-scale wave numbers and n small-scale wave numbers, to the n-point small-scale density correlation, with ℓ prefactors that involve the linear power spectrum at the large-scale wave numbers [17–25]. These relations, obtained at the leading order over the large-scale wave numbers k_j', arise from the equivalence principle, which ensures that small-scale structures respond to a large-scale perturbation (which at leading order corresponds to a constant gravitational force over the extent of the small-size object) by a uniform displacement. Therefore, these relations express a kinematic effect, due to the displacement of small-scale structures between different times. This also means that (at this order) they vanish for equal-time

statistics, as a uniform displacement has no impact on the statistical properties of the density field observed at a given time. Because they derive from the equivalence principle, these relations are very general and also apply to baryons and galaxies. However, in a standard cosmology, they provide no information at equal times (apart from constraining possible deviations from Gaussian initial conditions and general relativity).

To obtain nonvanishing results for equal-time statistics, one must go beyond this kinematic effect. This implies studying the response of small-scale structures to nonuniform gravitational forces, which at leading order and after averaging over angles correspond to a large-scale gravitational curvature. As proposed in Refs. [26] and [27], this is possible by using an approximate symmetry of the gravitational dynamics (associated with the common approximation $\Omega_{\rm m}/f^2 \simeq 1$, where $\Omega_{\rm m}$ is the matter density cosmological parameter and $f = {\rm d}\ln D_+/{\rm d}\ln a$ is the linear growth rate), which allows one to absorb the change of cosmological parameters (hence of the background curvature) by a change of variable. These relations again connect the $(\ell + n)$-point polyspectra, with ℓ large-scale modes and n small-scale modes, to the n-point polyspectrum, when an angular averaging operation is taken over the ℓ large-scale modes, which also removes the kinematic effect. These consistency relations no longer vanish at equal times, but they are less general than the previous relations. Indeed, galaxy formation processes (cooling, star formation, etc.) introduce new characteristic scales that would explicitly break this symmetry. The lowest-order relation, which applies to the matter bispectrum, has been explicitly tested in Ref. [28] using a large ensemble of cosmological N-body simulations; see also Refs. [29–31] for related discussions and comparisons with simulations or halo models.

The aim of this paper is to generalize this analysis, presented in Refs. [26] and [28] in real space, to redshift space, where actual observations take place. This is only a first step toward a comparison with measures from galaxy surveys, because we do not consider the important issue of galaxy bias in this paper (i.e., to translate our results in terms of the galaxy distribution, one would need to add a model that relates the galaxy and matter density fields). However, this remains a useful task as redshift-space statistics are well known to be difficult to model because small-scale nonperturbative effects have a non-negligible impact up to rather large scales [4,32,33], for instance, through the fingers-of-god effect [34]. Therefore, it is even more important than for real-space statistics to build tools that hold beyond the perturbative regime.

This paper is organized as follows. First, in Sec. II, we introduce the statistics of the redshift-space density field and its response to the initial conditions. Then, in Sec. III, we describe the dynamical equations of the system that we consider here and show their symmetry that is valid under the approximation $\Omega_{\rm m}/f^2 \simeq 1$. Using these results, we finally derive the angular-averaged consistency relations in Sec. IV. We focus on the lowest-order version of these relations, i.e., the bispectrum, in Sec. V, where we present our results in terms of the multipole moments of the spectra. We also introduce a simple *ansatz* to estimate new derivative terms in the relation from observables, to simplify its form and facilitate the connection with practical situations. In Sec. VI, the consistency relations are checked both perturbatively and nonperturbatively using analytical calculations. We then exploit numerical simulations to give a further test of the relations in Sec. VII. We finally summarize our findings in Sec. VIII.

II. MATTER DENSITY CORRELATIONS

In this paper, we assume that the nonlinear matter density contrast, $\delta(\boldsymbol{x}, t) = [\rho(\boldsymbol{x}, t) - \bar{\rho}]/\bar{\rho}$, is fully defined at any time by the initial linear density contrast δ_{L0} (i.e., decaying modes have had time to vanish) and that the latter is Gaussian and fully described by the linear power spectrum $P_{L0}(k)$,

$$\langle \tilde{\delta}_{L0}(\boldsymbol{k}_1)\tilde{\delta}_{L0}(\boldsymbol{k}_2)\rangle = P_{L0}(k_1)\delta_D(\boldsymbol{k}_1 + \boldsymbol{k}_2), \tag{1}$$

where we denote with a tilde Fourier-space fields. The matter density contrast can also be written in terms of the particle trajectories, $\boldsymbol{x}(\mathbf{q}, t)$, where $\mathbf{q}$ is the Lagrangian coordinate of the particles, as

$$k \neq 0 : \tilde{\delta}(\boldsymbol{k}, t) = \int \frac{{\rm d}\boldsymbol{x}}{(2\pi)^3} e^{-{\rm i}\boldsymbol{k}\cdot\boldsymbol{x}}\delta(\boldsymbol{x}, t) \tag{2}$$

$$= \int \frac{{\rm d}\mathbf{q}}{(2\pi)^3} e^{-{\rm i}\boldsymbol{k}\cdot\boldsymbol{x}(\mathbf{q},t)}, \tag{3}$$

where we discarded a Dirac term that does not contribute for $k \neq 0$. This expression follows from the conservation of matter, $\rho {\rm d}\boldsymbol{x} = \bar{\rho}{\rm d}\mathbf{q}$, which yields $[1 + \delta(\boldsymbol{x})]{\rm d}\boldsymbol{x} = {\rm d}\mathbf{q}$.

Using the Gaussianity of the linear density field δ_{L0}, integrations by parts allow us to write the correlation between ℓ linear fields and n nonlinear fields in terms of the response of the latter to changes of the initial conditions [23,26]

$$\langle \tilde{\delta}_{L0}(\boldsymbol{k}'_1)\ldots\tilde{\delta}_{L0}(\boldsymbol{k}'_\ell)\tilde{\delta}(\boldsymbol{k}_1, t_1)\ldots\tilde{\delta}(\boldsymbol{k}_n, t_n)\rangle$$
$$= P_{L0}(k'_1)\ldots P_{L0}(k'_\ell)\left\langle \frac{\mathcal{D}^\ell[\tilde{\delta}(\boldsymbol{k}_1, t_1)\ldots\tilde{\delta}(\boldsymbol{k}_n, t_n)]}{\mathcal{D}\tilde{\delta}_{L0}(-\boldsymbol{k}'_1)\ldots\mathcal{D}\tilde{\delta}_{L0}(-\boldsymbol{k}'_\ell)}\right\rangle. \tag{4}$$

This exact relation, which only relies on the Gaussianity of the initial condition $\tilde{\delta}_{L0}$, holds for any nonlinear field $\tilde{\delta}$, which is not necessarily identified with the nonlinear density contrast. It is also the basis of the consistency relations between $(\ell + n)$- and n-point polyspectra, in the limit $k'_j \to 0$, when one can write the right-hand side in

terms of $\langle\tilde{\delta}(\boldsymbol{k}_1,t_1)\ldots\tilde{\delta}(\boldsymbol{k}_n,t_n)\rangle$ multiplied by some deterministic prefactors or operators [17–23,26,27].

In this paper, we extend the analysis presented in Ref. [26] for the real-space density field to the redshift-space density field. Because of the Doppler effect associated with the peculiar velocities, the radial position of cosmological objects (e.g., galaxies) is not exactly given by their redshift, interpreted as a distance within the uniform background cosmology. For instance, receding objects appear to have a slightly higher redshift than the one associated with their actual location, and one is led to introduce the redshift-space coordinate $\boldsymbol{s}$ defined as [33,35,36]

$$\boldsymbol{s}=\boldsymbol{x}+\frac{v_r}{\dot{a}}\mathbf{e}_r, \tag{5}$$

where $\mathbf{e}_r$ is the radial unit vector along the line of sight (we use a plane-parallel approximation throughout this article), v_r is the line-of-sight component of the peculiar velocity $\boldsymbol{v}$, and $\dot{a}=\mathrm{d}a/\mathrm{d}t$ is the time derivative of the scale factor $a(t)$. Then, the redshift-space density contrast δ^s can be written in terms of the Lagrangian coordinate $\mathbf{q}$ of the particles as [33,36,37]

$$k\neq 0\colon\ \tilde{\delta}^s(\boldsymbol{k},t)=\int\frac{\mathrm{d}\mathbf{q}}{(2\pi)^3}e^{-\mathrm{i}\boldsymbol{k}\cdot\boldsymbol{s}(\mathbf{q},t)}, \tag{6}$$

where we again discarded a Dirac term that does not contribute for $k\neq 0$. This is the same expression as Eq. (3) for the real-space density contrast $\tilde{\delta}(\boldsymbol{k})$, except that $\boldsymbol{x}(\mathbf{q},t)$ in the exponential is replaced by $\boldsymbol{s}(\mathbf{q},t)$, and it again follows from the conservation of matter, $[1+\delta^s(\boldsymbol{s})]\mathrm{d}\boldsymbol{s}=\mathrm{d}\mathbf{q}$. Then, the redshift-space generalization of Eq. (4) reads as

$$\begin{aligned}&\langle\tilde{\delta}_{L0}(\boldsymbol{k}'_1)\ldots\tilde{\delta}_{L0}(\boldsymbol{k}'_\ell)\tilde{\delta}^s(\boldsymbol{k}_1,t_1)\ldots\tilde{\delta}^s(\boldsymbol{k}_n,t_n)\rangle\\&\quad=P_{L0}(k'_1)\ldots P_{L0}(k'_\ell)\left\langle\frac{\mathcal{D}^\ell[\tilde{\delta}^s(\boldsymbol{k}_1,t_1)\ldots\tilde{\delta}^s(\boldsymbol{k}_n,t_n)]}{\mathcal{D}\tilde{\delta}_{L0}(-\boldsymbol{k}'_1)\ldots\mathcal{D}\tilde{\delta}_{L0}(-\boldsymbol{k}'_\ell)}\right\rangle.\end{aligned} \tag{7}$$

As in Refs. [26,28], we focus on the relations obtained for $\ell=1$ by performing a spherical average over the angles of the large-scale wave number $\boldsymbol{k}'$. This removes the leading-order contribution, associated with a uniform displacement of small-scale structures by larger-scale modes, that vanishes for equal-time statistics ($t_1=\ldots=t_n$) [17–23]. One is left with the next-order contribution, which does not vanish at equal times [26–28] and is associated with the change to the growth of small-scale structures in a perturbed mean density background, modulated by the larger-scale modes. In configuration space, this means that we consider angular-averaged quantities of the form [26,28]

$$C_W^n=\int\mathrm{d}\boldsymbol{x}'W(x')\langle\delta_{L0}(\boldsymbol{x}')\delta^s(\boldsymbol{s}_1,t_1)\ldots\delta^s(\boldsymbol{s}_n,t_n)\rangle, \tag{8}$$

which read in Fourier space as

$$\tilde{C}_W^n=(2\pi)^3\int\mathrm{d}\boldsymbol{k}'\tilde{W}(k')\langle\tilde{\delta}_{L0}(\boldsymbol{k}')\tilde{\delta}^s(\boldsymbol{k}_1,t_1)\ldots\delta^s(\boldsymbol{k}_n,t_n)\rangle, \tag{9}$$

where $W(x')$ [and its Fourier transform $\tilde{W}(k')$] is a large-scale spherical window function. Using Eq. (7), we obtain

$$C_W^n=\left.\frac{\mathrm{d}}{\mathrm{d}\varepsilon_0}\right|_{\varepsilon_0=0}\langle\delta^s(\boldsymbol{s}_1,t_1)\ldots\delta^s(\boldsymbol{s}_n,t_n)\rangle_{\varepsilon_0} \tag{10}$$

and a similar relation for $\tilde{C}_W^n$, where $\langle\ldots\rangle_{\varepsilon_0}$ is the statistical average with respect to the Gaussian initial conditions δ_{L0}, when the linear density field is modified as

$$\delta_L(\boldsymbol{x})\to\delta_L(\boldsymbol{x})+\varepsilon_0 D_+(t)\int\mathrm{d}\boldsymbol{x}'W(x')C_{L0}(\boldsymbol{x},\boldsymbol{x}'), \tag{11}$$

where C_{L0} is the linear density contrast real-space correlation function. In the large-scale limit for the window function W, which corresponds to the limit $k'\to 0$, the integral over $\boldsymbol{x}'$ is independent of the position $\boldsymbol{x}$ in the small-scale region, at leading order in the ratio of scales, and the initial linear density contrast is merely shifted by a uniform amount,

$$k'\to 0\colon\ \Delta\delta_{L0}=\varepsilon_0\int\mathrm{d}\boldsymbol{x}'W(x')C_{L0}(x'). \tag{12}$$

This corresponds to a change of the background mean density $\bar{\rho}$, which means that we must obtain the impact of a small change of $\bar{\rho}$, and hence of cosmological parameters, on the small-scale correlation $\langle\delta^s(\boldsymbol{s}_1,t_1)\ldots\delta^s(\boldsymbol{s}_n,t_n)\rangle$.

III. APPROXIMATE SYMMETRY OF THE COSMOLOGICAL GRAVITATIONAL DYNAMICS

On scales much smaller than the horizon, where the Newtonian approximation is valid, the equations of motion read as [38]

$$\frac{\partial\delta}{\partial t}+\frac{1}{a}\nabla\cdot[(1+\delta)\boldsymbol{v}]=0, \tag{13}$$

$$\frac{\partial\boldsymbol{v}}{\partial t}+H\boldsymbol{v}+\frac{1}{a}(\boldsymbol{v}\cdot\nabla)\boldsymbol{v}=-\frac{1}{a}\nabla\phi, \tag{14}$$

$$\nabla^2\phi=4\pi\mathcal{G}\bar{\rho}a^2\delta. \tag{15}$$

Here, we use the single-stream approximation to simplify the presentation, but our results remain valid beyond shell crossing. Linearizing these equations over $\{\delta,\boldsymbol{v}\}$, one obtains the linear growth rates $D_\pm(t)$, which are the independent solutions of [4,38]

$$\ddot{D}+2H\dot{D}-4\pi\mathcal{G}\bar{\rho}D=0. \tag{16}$$

Then, it is convenient to make the change of variables [5,26,39,40]

$$\eta = \ln D_+, \qquad \boldsymbol{v} = \dot{a} f \mathbf{u}, \qquad \phi = (\dot{a} f)^2 \varphi, \quad (17)$$

with

$$f = \frac{\mathrm{d}\ln D_+}{\mathrm{d}\ln a} = \frac{a\dot{D}_+}{\dot{a} D_+}, \quad (18)$$

and the equations of motion read as

$$\frac{\partial \delta}{\partial \eta} + \nabla \cdot [(1+\delta)\mathbf{u}] = 0, \quad (19)$$

$$\frac{\partial \mathbf{u}}{\partial \eta} + \left(\frac{3\Omega_{\rm m}}{2f^2} - 1\right)\mathbf{u} + (\mathbf{u}\cdot\nabla)\mathbf{u} = -\nabla\varphi, \quad (20)$$

$$\nabla^2 \varphi = \frac{3\Omega_{\rm m}}{2f^2}\delta. \quad (21)$$

Here, $\Omega_{\rm m}(t)$ is the matter density cosmological parameter as a function of time, which obeys $4\pi\mathcal{G}\bar{\rho} = (3/2)\Omega_{\rm m}H^2$. As pointed out in Ref. [26], within the approximation $\Omega_{\rm m}/f^2 \simeq 1$ (which is used by most perturbative approaches [4]), all explicit dependence on cosmology disappears from the equations of motion (19)–(21). This means that the dependence of the density and velocity fields on cosmology is fully absorbed by the change of variable (17). Then, a change of the background density, as in Eq. (12), can be absorbed through a change of the time-dependent functions $\{a(t), D_+(t), f(t)\}$, which enter the change of variables (17) [26].

Here, we used the single-stream approximation to simplify the presentation, but the results remain valid beyond shell crossing, as the dynamics of particle trajectories, $\boldsymbol{x}(\mathbf{q}, t)$, follow the equation

$$\frac{\partial^2 \boldsymbol{x}}{\partial \eta^2} + \left(\frac{3\Omega_{\rm m}}{2f^2} - 1\right)\frac{\partial \boldsymbol{x}}{\partial \eta} = -\nabla\varphi, \quad (22)$$

where φ is the rescaled gravitational potential (21). This explicitly shows that they satisfy the same approximate symmetry. Therefore, our results are not restricted to the perturbative regime and also apply to small nonlinear scales governed by shell-crossing effects, as long as the approximation $\Omega_{\rm m}/f^2 \simeq 1$ is sufficiently accurate (but this also means that we are restricted to scales dominated by gravity).

IV. ANGULAR-AVERAGED CONSISTENCY RELATIONS

As described in Ref. [26], the impact of a small uniform change of the matter density background can be obtained by considering two universes with nearby background densities and scale factors, $\{\bar{\rho}(t), a(t)\}$ and $\{\bar{\rho}'(t), a'(t)\}$, with

$$\bar{\rho} a^3 = \bar{\rho}' a'^3 = \bar{\rho}_0, \qquad a' = a[1-\epsilon(t)],$$
$$\bar{\rho}' = \bar{\rho}[1+3\epsilon(t)]. \quad (23)$$

Here and in the following, we only keep terms up to linear order over ϵ. Then, writing the Friedmann equations for the two scale factors $a(t)$ and $a'(t)$ and linearizing over ϵ, we find that $\epsilon(t)$ must satisfy the same equation (16) as the linear growing mode [38]. Thus, we can write

$$\epsilon(t) = D_+(t)\epsilon_0. \quad (24)$$

For our purposes, the universe $\{\bar{\rho}(t), a(t)\}$ is the actual universe, with the zero-mean initial condition δ_{L0}, to which is added the uniform density perturbation (12). To recover zero-mean density fluctuations, we must shift the background by the same amount. Thus, this new background $\{\bar{\rho}'(t), a'(t)\}$ is given by

$$\epsilon_0 = \frac{1}{3}\Delta\delta_{L0} = \frac{\varepsilon_0}{3}\int \mathrm{d}x' W(x') C_{L0}(x'), \quad (25)$$

where we used the last relation (23), which gives, at linear order over δ and ϵ, $\delta_L = \delta'_L + 3\epsilon$.

Because both frames refer to the same physical system, we have $\mathbf{r}' = \mathbf{r} = a'\boldsymbol{x}' = a\boldsymbol{x}$, $\bar{\rho}'(1+\delta') = \bar{\rho}(1+\delta)$, where $\mathbf{r} = \mathbf{r}'$ is the physical coordinate. Thus, we have the relations

$$\boldsymbol{x}' = (1+\epsilon)\boldsymbol{x}, \qquad \delta' = \delta - 3\epsilon(1+\delta), \qquad \boldsymbol{v}' = \boldsymbol{v} + \dot{\epsilon} a \boldsymbol{x}, \quad (26)$$

where we used Eq. (23) and only kept terms up to linear order over ϵ. In particular, we can check that, if the fields $\{\delta', \boldsymbol{v}', \phi'\}$ satisfy the equations of motion (13)–(15) in the primed frame, the fields $\{\delta, \boldsymbol{v}, \phi\}$ satisfy the equations of motion (13)–(15) in the unprimed frame, with the gravitational potential transforming as $\phi' = \phi - a^2(\ddot{\epsilon} + 2H\dot{\epsilon})x^2/2$. This remains valid beyond the shell crossing; if the trajectories $\boldsymbol{x}'(\mathbf{q}, t)$ satisfy the equation of motion in the primed frame, the trajectories $\boldsymbol{x}(\mathbf{q}, t) = (1-\epsilon)\boldsymbol{x}'(\mathbf{q}, t)$ satisfy the equation of motion in the unprimed frame.

From the definition (5) and Eq. (26), we obtain the relation between the redshift-space coordinates,

$$\boldsymbol{s}' = (1+\epsilon)\boldsymbol{s} + \frac{\dot{\epsilon}}{H} s_r \mathbf{e}_r, \quad (27)$$

using $a' = (1-\epsilon)a$ and $H' = H - \dot{\epsilon}$. Then, using, for instance, the expressions (3) and (6), the real-space and the redshift-space density contrasts in the actual unprimed frame, with the uniform overdensity $\Delta\delta_{L0} = 3\epsilon_0$, can be written as [26]

$$k \neq 0\colon \tilde{\delta}_{\epsilon_0}(\boldsymbol{k}, t) = \tilde{\delta}[(1-\epsilon)\boldsymbol{k}, D_{+\epsilon_0}] \quad (28)$$

and

$$\tilde{\delta}^s_{\epsilon_0}(\boldsymbol{k}, t) = \tilde{\delta}^s\left[(1-\epsilon)\boldsymbol{k} - \frac{\dot{\epsilon}}{H} k_r \mathbf{e}_r, D_{+\epsilon_0}, f_{\epsilon_0}\right], \quad (29)$$

where we disregarded a Dirac factor $\delta_D(\boldsymbol{k})$ that does not contribute for $k \neq 0$. In Eqs. (28) and (29), the subscript ϵ_0 recalls that we consider the formation of large-scale structures in the actual universe to which is added the small uniform overdensity $\Delta\delta_{L0} = 3\epsilon_0$.

The physical meaning of the expression (28) directly follows from the mapping (26) and the independence on cosmology of the equations of motion (19)–(21), within the approximation $\Omega_{\rm m}/f^2 \simeq 1$. It means that in the primed universe, with the slightly higher background density $\bar{\rho}' = (1+3\epsilon)\bar{\rho}$ (focusing, for instance, on the case $\epsilon > 0$), comoving distances $\boldsymbol{x}'$ show the small isotropic dilatation (26) [because the higher background density yields a higher gravitational force and a smaller scale factor $a'(t)$], whence an isotropic contraction of wave numbers $\boldsymbol{k}'$, while the linear growth factor $D_+(t)$ is also modified. Moreover, the approximate symmetry discussed in Sec. III implies that all time and cosmological dependence can be absorbed through the time coordinate D_+, if we work with the rescaled field $\{\delta, \mathbf{u}, \varphi\}$ of Eq. (17). This is denoted by the rescaled time coordinate $D_{+\epsilon_0}$ in the right-hand side of Eq. (28), where the subscript ϵ_0 recalls that we must take into account the impact of the modified background onto the linear growth factor.

For the redshift-space density contrast (29), two new effects arise, as compared with the real-space density contrast (28). First, the mapping $\boldsymbol{s} \leftrightarrow \boldsymbol{s}'$ is no longer isotropic because of the peculiar velocity component along the line of sight, see Eq. (27), which also leads to an anisotropic relationship $\boldsymbol{k} \leftrightarrow \boldsymbol{k}'$. Second, in addition to the time coordinate D_+, the redshift-space density contrast involves the new quantity $f(t)$. This follows from the definition (5), which can be written in terms of the rescaled velocity field $\mathbf{u}$ of Eq. (17) as

$$\boldsymbol{s} = \boldsymbol{x} + \frac{v_r}{\dot{a}}\mathbf{e}_r = \boldsymbol{x} + f u_r \mathbf{e}_r. \tag{30}$$

This shows that, in addition to the rescaled term u_r, which only depends on time and cosmology through the time coordinate D_+, within the approximate symmetry of Sec. III, the line-of-sight component explicitly involves a time- and cosmology-dependent factor $f(t)$, which must be taken into account in Eq. (29).

Then, to derive the angular-averaged consistency relations through Eq. (10), we simply need to use Eq. (29) to obtain the derivative of the redshift-space density contrast with respect to ϵ_0 and next to use Eq. (25). This yields

$$\frac{\partial\tilde{\delta}^s(\boldsymbol{k})}{\partial\epsilon_0} = \frac{\partial D_{+\epsilon_0}}{\partial\epsilon_0}\frac{\partial\tilde{\delta}^s}{\partial D_+} + \frac{\partial f_{\epsilon_0}}{\partial\epsilon_0}\frac{\partial\tilde{\delta}^s}{\partial f} - D_+(t)\boldsymbol{k}\cdot\frac{\partial\tilde{\delta}^s}{\partial\boldsymbol{k}} - fD_+k_r\frac{\partial\tilde{\delta}^s}{\partial k_r}, \tag{31}$$

where we disregarded a Dirac factor that does not contribute for wave numbers $\boldsymbol{k} \neq 0$.

As found in Refs. [26,41], the derivative of the linear growth factor reads as

$$\left.\frac{\partial D_{+\epsilon_0}}{\partial\epsilon_0}\right|_{\epsilon_0=0} = \frac{13}{7}D_+(t)^2. \tag{32}$$

This corresponds to $D'_+ = D_+ + (13/7)D_+^2\epsilon_0$ for the linear growing mode in the primed frame, while $a' = a - D_+a\epsilon_0$ and $H' = H - \dot{D}_+\epsilon_0$. From the definition (18), we obtain $f' = f + f(13/7D_+ + \dot{D}_+/H)\epsilon_0$, whence

$$\left.\frac{\partial f_{\epsilon_0}}{\partial\epsilon_0}\right|_{\epsilon_0=0} = fD_+\left(\frac{13}{7}+f\right). \tag{33}$$

Therefore, Eq. (31) gives

$$\frac{\partial\tilde{\delta}^s(\boldsymbol{k})}{\partial\epsilon_0} = \frac{13}{7}D_+(t)^2\frac{\partial\tilde{\delta}^s}{\partial D_+} + fD_+\left(\frac{13}{7}+f\right)\frac{\partial\tilde{\delta}^s}{\partial f} - D_+(t)\boldsymbol{k}\cdot\frac{\partial\tilde{\delta}^s}{\partial\boldsymbol{k}} - fD_+k_r\frac{\partial\tilde{\delta}^s}{\partial k_r}. \tag{34}$$

Of course, when we set f to zero, we recover the expression of the derivative with respect to ϵ_0 of the real-space density contrast $\tilde{\delta}$ [26]. In configuration space, this reads as

$$\frac{\partial\delta^s(\boldsymbol{s})}{\partial\epsilon_0} = D_+\left[\frac{13}{7}\frac{\partial}{\partial\ln D_+} + \left(\frac{13}{7}+f\right)f\frac{\partial}{\partial f} + 3 + f + \boldsymbol{s}\cdot\frac{\partial}{\partial\boldsymbol{s}} + fs_r\frac{\partial}{\partial s_r}\right]\delta^s(\boldsymbol{s}). \tag{35}$$

Next, from Eqs. (10) and (25), we obtain as for the real-space correlations [26]

$$C_W^n = \int \mathrm{d}\boldsymbol{x}' W(x')C_{L0}(x')\sum_{i=1}^{n}\frac{D_{+i}}{3}\left[3 + f_i + \frac{13}{7}\frac{\partial}{\partial\ln D_{+i}} + \left(\frac{13}{7}+f_i\right)f_i\frac{\partial}{\partial f_i} + \left(\boldsymbol{s}_i - \frac{1}{n}\sum_{j=1}^{n}\boldsymbol{s}_j\right)\cdot\frac{\partial}{\partial\boldsymbol{s}_i} + f_i\left(s_{ri} - \frac{1}{n}\sum_{j=1}^{n}s_{rj}\right)\frac{\partial}{\partial s_{ri}}\right]\langle\delta^s(\boldsymbol{s}_1,t_1)\ldots\delta(\boldsymbol{s}_n,t_n)\rangle. \tag{36}$$

The counterterms of the form $-1/n\sum_j\boldsymbol{s}_j$ ensure that all expressions are invariant with respect to uniform translations [by explicitly setting the small-scale region at the center of the large-scale perturbation (11)]. They are irrelevant for equal-time statistics, $t_1 = \ldots = t_n$, where factors of the form $\sum_i\boldsymbol{s}_i\cdot\frac{\partial}{\partial\boldsymbol{s}_i}\langle\tilde{\delta}_1^s\ldots\tilde{\delta}_n^s\rangle$ are already invariant with respect to uniform translations.

The comparison with Eq. (8) gives, after writing the correlations in terms of Fourier-space polyspectra,

$$\int \frac{\mathrm{d}\Omega_{\boldsymbol{k}'}}{4\pi} \langle \tilde{\delta}_{L0}(\boldsymbol{k}')\tilde{\delta}^s(\boldsymbol{k}_1,t_1)\ldots\tilde{\delta}^s(\boldsymbol{k}_n,t_n)\rangle'_{k'\to 0} = P_{L0}(k')\sum_{i=1}^{n} D_{+i}\left[\frac{1}{n}+\frac{f_i}{3n}+\frac{13}{21}\frac{\partial}{\partial \ln D_{+i}}+\left(\frac{13}{7}+f_i\right)\frac{f_i}{3}\frac{\partial}{\partial f_i}\right.$$
$$\left.-\sum_{j=1}^{n}\left(\delta^K_{i,j}-\frac{1}{n}\right)\frac{\boldsymbol{k}_i}{3}\cdot\frac{\partial}{\partial \boldsymbol{k}_j}-f_i\sum_{j=1}^{n}\left(\delta^K_{i,j}-\frac{1}{n}\right)\frac{k_{ri}}{3}\frac{\partial}{\partial k_{rj}}\right]\langle\tilde{\delta}^s(\boldsymbol{k}_1,t_1)\ldots\tilde{\delta}^s(\boldsymbol{k}_n,t_n)\rangle', \tag{37}$$

where $\Omega_{\boldsymbol{k}'}$ is the unit vector along the direction of $\boldsymbol{k}'$ and $\delta^K_{i,j}$ is the Kronecker symbol. The subscript $k'\to 0$ recalls that this relation only gives the leading-order term in the large-scale limit $k'\to 0$, whereas the wave numbers $\{\boldsymbol{k}_1,\ldots,\boldsymbol{k}_n\}$ are fixed and may be within the nonlinear regime. Here, we denoted with a prime the reduced polyspectra, defined as

$$\langle\tilde{\delta}^s(\boldsymbol{k}_1)\ldots\tilde{\delta}^s(\boldsymbol{k}_n)\rangle = \langle\tilde{\delta}^s(\boldsymbol{k}_1)\ldots\tilde{\delta}^s(\boldsymbol{k}_n)\rangle'\delta_D(\boldsymbol{k}_1+\ldots+\boldsymbol{k}_n), \tag{38}$$

where we explicitly factor out the Dirac factor associated with statistical homogeneity. In particular, this means that $\langle\tilde{\delta}^s(\boldsymbol{k}_1)\ldots\tilde{\delta}^s(\boldsymbol{k}_n)\rangle'$ can be written as a function of the $n-1$ wave numbers $\{\boldsymbol{k}_1,\ldots,\boldsymbol{k}_{n-1}\}$ only.

On large scales, we recover the linear theory [4,35], with $\tilde{\delta}(\boldsymbol{k}',t')\simeq D_+(t')\tilde{\delta}_{L0}(\boldsymbol{k}')$ and $\tilde{\delta}^s(\boldsymbol{k}',t')\simeq D_+(t')\tilde{\delta}_{L0}(\boldsymbol{k}')\times(1+f'\mu'^2)$, where μ' is the cosine of the wave number $\boldsymbol{k}'$ with the line of sight, as in

$$\mu = \frac{\boldsymbol{k}\cdot\mathbf{e}_r}{k}. \tag{39}$$

Therefore, Eq. (37) also gives

$$\int \frac{\mathrm{d}\Omega_{\boldsymbol{k}'}}{4\pi}\left\langle\frac{\tilde{\delta}^s(\boldsymbol{k}',t')}{1+f'\mu'^2}\tilde{\delta}^s(\boldsymbol{k}_1,t_1)\ldots\tilde{\delta}^s(\boldsymbol{k}_n,t_n)\right\rangle'_{k'\to 0} = P_L(k',t')\sum_{i=1}^{n}\frac{D_{+i}}{D'_+}\left[\frac{1}{n}+\frac{f_i}{3n}+\frac{13}{21}\frac{\partial}{\partial \ln D_{+i}}+\left(\frac{13}{7}+f_i\right)\frac{f_i}{3}\frac{\partial}{\partial f_i}\right.$$
$$\left.-\sum_{j=1}^{n}\left(\delta^K_{i,j}-\frac{1}{n}\right)\frac{\boldsymbol{k}_i}{3}\cdot\frac{\partial}{\partial \boldsymbol{k}_j}-f_i\sum_{j=1}^{n}\left(\delta^K_{i,j}-\frac{1}{n}\right)\frac{k_{ri}}{3}\frac{\partial}{\partial k_{rj}}\right]\langle\tilde{\delta}^s(\boldsymbol{k}_1,t_1)\ldots\tilde{\delta}^s(\boldsymbol{k}_n,t_n)\rangle'. \tag{40}$$

When all times are equal, $t'=t_1=\ldots=t_n\equiv t$, this simplifies as

$$\int \frac{\mathrm{d}\Omega_{\boldsymbol{k}'}}{4\pi}\left\langle\frac{\tilde{\delta}^s(\boldsymbol{k}')}{1+f\mu'^2}\tilde{\delta}^s(\boldsymbol{k}_1)\ldots\tilde{\delta}^s(\boldsymbol{k}_n)\right\rangle'_{k'\to 0} = P_L(k')\left[1+\frac{f}{3}+\frac{13}{21}\frac{\partial}{\partial \ln D_+}+\left(\frac{13}{7}+f\right)\frac{f}{3}\frac{\partial}{\partial f}\right.$$
$$\left.-\sum_{i=1}^{n}\frac{k_i}{3}\frac{\partial}{\partial k_i}-f\sum_{i=1}^{n}\frac{k_{ri}}{3}\frac{\partial}{\partial k_{ri}}\right]\langle\tilde{\delta}^s(\boldsymbol{k}_1)\ldots\tilde{\delta}^s(\boldsymbol{k}_n)\rangle'. \tag{41}$$

V. BISPECTRUM

A. Relation in $\{k,\mu^2\}$ space

The lowest-order equal-time consistency relation obtained from Eq. (41) corresponds to $n=2$, that is, the bispectrum built from the correlation between two small-scale modes and one large-scale mode. We define the bispectrum as in Eq. (38),

$$\langle\tilde{\delta}^s(\boldsymbol{k}_1)\tilde{\delta}^s(\boldsymbol{k}_1)\tilde{\delta}^s(\boldsymbol{k}_1)\rangle = B^s(\boldsymbol{k}_1,\boldsymbol{k}_2,\boldsymbol{k}_3)\delta_D(\boldsymbol{k}_1+\boldsymbol{k}_2+\boldsymbol{k}_3). \tag{42}$$

In contrast with the real-space bispectrum, $B(k_1,k_2,k_3)$, which only depends on the lengths of the three wave numbers $\{\boldsymbol{k}_1,\boldsymbol{k}_2,\boldsymbol{k}_3\}$ thanks to statistical isotropy, the redshift-space bispectrum also depends on angles because the velocity component along the line of sight breaks the isotropy. Then, Eq. (41) yields

$$\int\frac{\mathrm{d}\Omega_{\boldsymbol{k}'}}{4\pi}\frac{B^s(\boldsymbol{k}',\boldsymbol{k}-\boldsymbol{k}'/2,-\boldsymbol{k}-\boldsymbol{k}'/2)_{k'\to 0}}{1+f\mu'^2}$$
$$= P_L(k')\left[1+\frac{f}{3}+\frac{13}{21}\frac{\partial}{\partial \ln D_+}+\left(\frac{13}{7}+f\right)\frac{f}{3}\frac{\partial}{\partial f}\right.$$
$$\left.-\frac{1+f\mu^2}{3}\frac{\partial}{\partial \ln k}-\frac{f}{3}2\mu^2(1-\mu^2)\frac{\partial}{\partial\mu^2}\right]P^s(k,\mu^2). \tag{43}$$

Here, we used the symmetries of the redshift-space power spectrum to write $P^s(\boldsymbol{k})$ as a function of k and μ^2. In Eq. (43), the power spectrum is written as a function of time through the functions D_+ and f, that is,

$$P^s(\boldsymbol{k};t) = P^s(k,\mu^2;D_+,f). \tag{44}$$

In particular, in the linear regime, we have the well-known expression

$$P^s_L(\boldsymbol{k};t) = D_+^2 P_{L0}(k)(1+f\mu^2)^2, \tag{45}$$

where P_{L0} is the linear real-space power spectrum today. When $f=0$, the relation (43) recovers the real-space consistency relation, as it should.

B. Multipole expansion

The consistency relation (43) is written for a given value of k and μ. In practice, rather than considering the redshift-space power spectrum over a grid of μ, one often expands the dependence on μ over Legendre polynomials. Thus, we write the nonlinear redshift-space power spectrum as

$$P^s(\boldsymbol{k}) = P^s(k,\mu^2) = \sum_{\ell=0}^{\infty} P^s_{2\ell}(k) L_{2\ell}(\mu), \tag{46}$$

where $L_\ell(\mu)$ is the Legendre polynomial of order ℓ. Only even orders contribute to this expansion because P^s is an even function of μ. Substituting into Eq. (43), we obtain

$$\begin{aligned}
&\frac{4\ell+1}{2}\int_{-1}^{1} d\mu L_{2\ell}(\mu) \int \frac{d\Omega_{\boldsymbol{k}'}}{4\pi} \frac{B^s(\boldsymbol{k}', \boldsymbol{k}-\frac{\boldsymbol{k}'}{2}, -\boldsymbol{k}-\frac{\boldsymbol{k}'}{2})_{k'\to 0}}{1+f\mu'^2} \\
&= P_L(k')\Bigg\{\left[1+\frac{f}{3}+\frac{13}{21}\frac{\partial}{\partial \ln D_+}+\left(\frac{13}{7}+f\right)\frac{f}{3}\frac{\partial}{\partial f}-\frac{1}{3}\frac{\partial}{\partial \ln k}\right]P^s_{2\ell}(k) - \frac{f}{3}\frac{\partial}{\partial \ln k}\left[\frac{(2\ell-1)2\ell}{(4\ell-3)(4\ell-1)}P^s_{2\ell-2}\right. \\
&\quad \left. + \frac{(8\ell^2+4\ell-1)}{(4\ell-1)(4\ell+3)}P^s_{2\ell} + \frac{(2\ell+1)(2\ell+2)}{(4\ell+3)(4\ell+5)}P^s_{2\ell+2}\right] - \frac{f}{3}\left[-\frac{(2\ell-2)(2\ell-1)2\ell}{(4\ell-3)(4\ell-1)}P^s_{2\ell-2} + \frac{(2\ell(2\ell+1)}{(4\ell-1)(4\ell+3)}P^s_{2\ell}\right. \\
&\quad \left. + \frac{(2\ell+1)(2\ell+2)(2\ell+3)}{(4\ell+3)(4\ell+5)}P^s_{2\ell+2}\right]\Bigg\}.
\end{aligned} \tag{47}$$

For the first two multipoles, $2\ell=0$ and $2\ell=2$, this yields

$$\begin{aligned}
\int_{-1}^{1}\frac{d\mu}{2}\int\frac{d\Omega_{\boldsymbol{k}'}}{4\pi}\frac{B^s_{k'\to 0}}{1+f\mu'^2} &= P_L(k')\Bigg\{\left[1+\frac{f}{3}+\frac{13}{21}\frac{\partial}{\partial \ln D_+}+\left(\frac{13}{7}+f\right)\frac{f}{3}\frac{\partial}{\partial f}-\frac{1}{3}\frac{\partial}{\partial \ln k}\right]P^s_0(k) - \frac{2f}{15}P^s_2(k) \\
&\quad - \frac{f}{3}\frac{\partial}{\partial \ln k}\left[\frac{1}{3}P^s_0(k)+\frac{2}{15}P^s_2(k)\right]\Bigg\}
\end{aligned} \tag{48}$$

and

$$\begin{aligned}
\frac{5}{2}\int_{-1}^{1} d\mu L_2(\mu)\int\frac{d\Omega_{\boldsymbol{k}'}}{4\pi}\frac{B^s_{k'\to 0}}{1+f\mu'^2} &= P_L(k')\Bigg\{\left[1+\frac{f}{3}+\frac{13}{21}\frac{\partial}{\partial \ln D_+}+\left(\frac{13}{7}+f\right)\frac{f}{3}\frac{\partial}{\partial f}-\frac{1}{3}\frac{\partial}{\partial \ln k}\right]P^s_2(k) \\
&\quad - \frac{f}{3}\frac{\partial}{\partial \ln k}\left[\frac{2}{3}P^s_0(k)+\frac{11}{21}P^s_2(k)+\frac{4}{21}P^s_4(k)\right] - \frac{f}{3}\left[\frac{2}{7}P^s_2(k)+\frac{20}{21}P^s_4(k)\right]\Bigg\}.
\end{aligned} \tag{49}$$

C. f derivative

1. Relations in $\{k,\mu^2\}$ space

In practice, we cannot directly measure the derivative with respect to f of the redshift-space power spectrum because the time derivative combines the derivatives with respect to D_+ and f. Therefore, the expression (43) can only be applied to analytical models, where the dependences on D_+ and f are explicitly known. To obtain an expression that can be applied to numerical or observed power spectra, we must write the derivative with respect to f in terms of observed time or space coordinates. Since the redshift-space power spectrum must coincide with the real-space power spectrum when either f or μ^2 vanishes, each factor f (respectively, μ^2) must appear in combination with a power of μ^2 (respectively, f). Here, we make the *ansatz* that the dependence on f and μ^2 only appears through the combination $f\mu^2$, which is exact at the linear order (45) (but

at higher-order terms of the form $f\mu^4, f\mu^6, ...$, might appear). This gives

$$P^s(\boldsymbol{k},t) = P^s(k, f\mu^2; D_+) \quad \text{implies } f\frac{\partial P^s}{\partial f} = \mu^2 \frac{\partial P^s}{\partial \mu^2}. \tag{50}$$

This allows us to write Eq. (43) as

$$\int \frac{\mathrm{d}\Omega_{\boldsymbol{k}'}}{4\pi} \frac{B^s(\boldsymbol{k}', \boldsymbol{k}-\boldsymbol{k}'/2, -\boldsymbol{k}-\boldsymbol{k}'/2)}{1+f\mu'^2} = P_L(k')\left[1 + \frac{f}{3} + \frac{13}{21}\frac{\partial}{\partial \ln D_+} - \frac{1+f\mu^2}{3}\frac{\partial}{\partial \ln k} + \left(\frac{13}{7} - f + 2f\mu^2\right)\frac{\mu^2}{3}\frac{\partial}{\partial \mu^2}\right] P^s(k, f\mu^2; D_+). \tag{51}$$

In practice, we only measure the dependence of the power spectrum with respect to time t, or scale factor $a(t)$, and wave number coordinates $\{k, \mu\}$. Then, writing $\partial/\partial t = \dot{D}_+ \partial/\partial D_+ + \dot{f}\partial/\partial f$ and using Eq. (50), we obtain

$$\frac{\partial P^s}{\partial \ln D_+} = \frac{1}{f}\left[\frac{\partial P^s}{\partial \ln a} - \frac{a\dot{f}}{\dot{a}f}\mu^2 \frac{\partial P^s}{\partial \mu^2}\right], \tag{52}$$

which gives

$$\int \frac{\mathrm{d}\Omega_{\boldsymbol{k}'}}{4\pi} \frac{B^s(\boldsymbol{k}', \boldsymbol{k}-\boldsymbol{k}'/2, -\boldsymbol{k}-\boldsymbol{k}'/2)}{1+f\mu'^2} = P_L(k')\left[1 + \frac{f}{3} + \frac{13}{21f}\frac{\partial}{\partial \ln a} - \frac{1+f\mu^2}{3}\frac{\partial}{\partial \ln k} + \left(\frac{13}{7} - f + 2f\mu^2 - \frac{13a\dot{f}}{7\dot{a}f^2}\right)\frac{\mu^2}{3}\frac{\partial}{\partial \mu^2}\right] P^s(k, \mu^2; a). \tag{53}$$

Using the approximation $\Omega_\mathrm{m}/f^2 \simeq 1$, we might simplify Eq. (53) by writing $\dot{f} \simeq \frac{\dot{D}_+}{D_+}[-2 + f/2 + 3f^2/2]$. However, this introduces an additional source of error, and at redshift $z = 0.35$, this gives a 15% error on $\dot{f}$. We checked numerically that this can lead to violations of the consistency relations by factors as large as 3 or as small as 0.5. Therefore, we keep the expression (53) in the following. [The impact of the approximation $\Omega_\mathrm{m}/f^2 \simeq 1$ is greater on the explicit factor $\dot{f}$ in Eq. (53) than on the consistency relation itself, which also relied on this approximation, because the factor $\dot{f}$ is evaluated at the observed redshift, whereas the consistency relation involves the behavior of the growing modes over all previous redshifts, following the growth of density fluctuations, which damps the impact of late-time behaviors.]

2. Multipole expansions

We can again write the relations (51) and (53) in terms of the multipole expansion (46). For the first two multipoles, Eq. (51) leads to

$$\int_{-1}^{1}\frac{\mathrm{d}\mu}{2}\int \frac{\mathrm{d}\Omega_{\boldsymbol{k}'}}{4\pi}\frac{B^s_{\boldsymbol{k}'\to 0}}{1+f\mu'^2} = P_L(k')\left\{\left[1 + \frac{f}{3} + \frac{13}{21}\frac{\partial}{\partial \ln D_+} - \frac{1}{3}\frac{\partial}{\partial \ln k}\right]P^s_0(k) - \frac{f}{3}\frac{\partial}{\partial \ln k}\left[\frac{1}{3}P^s_0(k) + \frac{2}{15}P^s_2(k)\right] + \frac{65+7f}{210}P^s_2(k) + \frac{13+7f}{42}\sum_{\ell=2}^{\infty}P^s_{2\ell}(k)\right\} \tag{54}$$

and

$$\frac{5}{2}\int_{-1}^{1}\mathrm{d}\mu L_2(\mu)\int \frac{\mathrm{d}\Omega_{\boldsymbol{k}'}}{4\pi}\frac{B^s_{\boldsymbol{k}'\to 0}}{1+f\mu'^2} = P_L(k')\left\{\left[1 + \frac{f}{3} + \frac{13}{21}\frac{\partial}{\partial \ln D_+} - \frac{1}{3}\frac{\partial}{\partial \ln k}\right]P^s_2(k) - \frac{f}{3}\frac{\partial}{\partial \ln k}\left[\frac{2}{3}P^s_0(k) + \frac{11}{21}P^s_2(k) + \frac{4}{21}P^s_4(k)\right] + \frac{13+5f}{21}P^s_2(k) + \frac{195+65f}{126}P^s_4(k) + \frac{65+35f}{42}\sum_{\ell=3}^{\infty}P^s_{2\ell}(k)\right\}, \tag{55}$$

while Eq. (53) leads to

$$\int_{-1}^{1}\frac{\mathrm{d}\mu}{2}\int \frac{\mathrm{d}\Omega_{\boldsymbol{k}'}}{4\pi}\frac{B^s_{\boldsymbol{k}'\to 0}}{1+f\mu'^2} = P_L(k')\left\{\left[1 + \frac{f}{3} + \frac{13}{21f}\frac{\partial}{\partial \ln a} - \frac{1}{3}\frac{\partial}{\partial \ln k}\right]P^s_0(k) - \frac{f}{3}\frac{\partial}{\partial \ln k}\left[\frac{1}{3}P^s_0(k) + \frac{2}{15}P^s_2(k)\right] + \left(\frac{13}{42} + \frac{f}{30} - \frac{13a\dot{f}}{42\dot{a}f^2}\right)P^s_2(k) + \left(\frac{13}{42} + \frac{f}{6} - \frac{13a\dot{f}}{42\dot{a}f^2}\right)\sum_{\ell=2}^{\infty}P^s_{2\ell}(k)\right\} \tag{56}$$

and

$$\frac{5}{2}\int_{-1}^{1}\mathrm{d}\mu L_2(\mu)\int\frac{\mathrm{d}\Omega_{\boldsymbol{k}'}}{4\pi}\frac{B^s_{k'\to 0}}{1+f\mu'^2}=P_L(k')\left\{\left[1+\frac{f}{3}+\frac{13}{21f}\frac{\partial}{\partial\ln a}-\frac{1}{3}\frac{\partial}{\partial\ln k}\right]P^s_2(k)\right.$$
$$-\frac{f}{3}\frac{\partial}{\partial\ln k}\left[\frac{2}{3}P^s_0(k)+\frac{11}{21}P^s_2(k)+\frac{4}{21}P^s_4(k)\right]$$
$$+\left(\frac{13}{21}+\frac{5f}{21}-\frac{13a\dot{f}}{21\dot{a}f^2}\right)P^s_2(k)+\left(\frac{65}{42}+\frac{65f}{126}-\frac{65a\dot{f}}{42\dot{a}f^2}\right)P^s_4(k)$$
$$\left.+\left(\frac{65}{42}+\frac{5f}{6}-\frac{65a\dot{f}}{42\dot{a}f^2}\right)\sum_{\ell=3}^{\infty}P^s_{2\ell}(k)\right\}. \tag{57}$$

As compared with Eqs. (48) and (49), these relations involve all multipoles $P^s_{2\ell}$ in the right-hand sides because the substitution (50) gives rise to factors $\mu^2\partial/\partial\mu^2$ rather than the factor $(1-\mu^2)\partial/\partial\mu^2$ that appeared in Eq. (43). In practice, it is not possible to measure or compute all multipoles, and one must truncate these multipole series at some order $\ell_{\max}$. This implies an additional approximation onto these relations (54)–(57).

VI. EXPLICIT CHECKS

The angular-averaged consistency relations (37)–(41) are valid at all orders of perturbation theory and also beyond the perturbative regime, including shell-crossing effects, within the accuracy of the approximation $\Omega_{\mathrm{m}}/f^2\simeq 1$ (and as long as gravity is the dominant process).

We now provide two explicit checks of the angular-averaged consistency relations (37)–(41). First, we check these relations for the lowest-order case $n=2$, that is, for the bispectrum, at the lowest order of perturbation theory. Second, we present a fully nonlinear and nonperturbative check, for arbitrary n-point polyspectra, in the one-dimensional case.

A. Perturbative check

Here, we briefly check the consistency relations for the lowest-order case, $n=2$, given by Eq. (43) at equal times, at the lowest order of perturbation theory. At this order, the equal-time redshift-space matter density bispectrum reads as [4]

$$B^s(\boldsymbol{k}_1,\boldsymbol{k}_2,\boldsymbol{k}_3)=2D_+^4P_{L0}(k_1)P_{L0}(k_2)Z_1(\boldsymbol{k}_1)Z_1(\boldsymbol{k}_2)\times Z_2(\boldsymbol{k}_1,\boldsymbol{k}_2)+2\,\mathrm{perm}, \tag{58}$$

where "2 perm." stands for two other terms that are obtained from permutations over the indices $\{1,2,3\}$ and the kernels Z_1 and Z_2 are given by

$$Z_1(\boldsymbol{k})=1+f\mu^2 \tag{59}$$

and

$$Z_2(\boldsymbol{k}_1,\boldsymbol{k}_2)=\frac{5+3f\mu^2}{7}+\frac{1+f\mu^2}{2}\left(\frac{k_1}{k_2}+\frac{k_2}{k_1}\right)\frac{\boldsymbol{k}_1\cdot\boldsymbol{k}_2}{k_1k_2}+\frac{2+4f\mu^2}{7}\left(\frac{\boldsymbol{k}_1\cdot\boldsymbol{k}_2}{k_1k_2}\right)^2+\frac{fk\mu}{2}\left[\frac{\mu_1}{k_1}(1+f\mu_2^2)+\frac{\mu_2}{k_2}(1+f\mu_1^2)\right], \tag{60}$$

where $\boldsymbol{k}=\boldsymbol{k}_1+\boldsymbol{k}_2$. In the small-$k'$ limit, we obtain

$$B^s_{k'\to 0}=2D_+^4P_{L0}(k')P_{L0}(k_1)Z_1(\boldsymbol{k}')Z_1(\boldsymbol{k}_1)Z_2(\boldsymbol{k}',\boldsymbol{k}_1)+(\boldsymbol{k}_1\leftrightarrow\boldsymbol{k}_2), \tag{61}$$

with $\boldsymbol{k}_1=\boldsymbol{k}-\boldsymbol{k}'/2$ and $\boldsymbol{k}_2=-\boldsymbol{k}-\boldsymbol{k}'/2$. Here, we used the fact that $Z_2(\boldsymbol{k}_1,\boldsymbol{k}_2)$ vanishes as $|\boldsymbol{k}_1+\boldsymbol{k}_2|^2$ for $|\boldsymbol{k}_1+\boldsymbol{k}_2|\to 0$, whereas $P_{L0}(k)\sim k^{n_s}$ with $n_s\lesssim 1$. [If this is not the case, that is, there is very little initial power on large scales, we must go back to the consistency relation in the form of Eq. (37) rather than Eq. (40). However, this is not necessary in realistic models.] Expanding the various terms over k', as

$$P_{L0}(k_1)=P_{L0}(k)-\frac{\boldsymbol{k}\cdot\boldsymbol{k}'}{2k}\frac{\mathrm{d}P_{L0}}{\mathrm{d}k}(k)+\cdots, \tag{62}$$

$$Z_1(\boldsymbol{k}_1)=1+f\mu^2-f\frac{k'}{k}\mu\mu'+f\mu^2\frac{\boldsymbol{k}\cdot\boldsymbol{k}'}{k^2}+\cdots, \tag{63}$$

$$Z_2(\boldsymbol{k}',\boldsymbol{k}_1)=\frac{13+19f\mu^2}{28}+\frac{4+f\mu^2}{14}\left(\frac{\boldsymbol{k}\cdot\boldsymbol{k}'}{kk'}\right)^2+(1+f\mu^2)\times\left[\frac{f\mu'^2}{4}+\frac{f\mu\mu'}{2}\frac{\boldsymbol{k}\cdot\boldsymbol{k}'}{kk'}+\frac{\boldsymbol{k}\cdot\boldsymbol{k}'}{2k'^2}+\frac{f\mu\mu'}{2}\frac{k}{k'}\right]+\cdots; \tag{64}$$

substituting into Eq. (61); and integrating over the angles of $\boldsymbol{k}'$, we obtain

$$\int \frac{d\Omega_{k'}}{4\pi}\frac{B^s_{k'\to 0}}{1+f\mu'^2} = P_L(k')P_L(k)(1+f\mu^2)\left[\frac{47}{21}+\frac{f}{3} + \frac{73f\mu^2}{21}-\frac{f^2\mu^2}{3}+\frac{4f^2\mu^4}{3}\right] - P_L(k')\frac{dP_L(k)}{d\ln k}\frac{(1+f\mu^2)^3}{3}. \quad (65)$$

On the other hand, the right-hand side of Eq. (43) reads at the same order over P_L as

$$\int \frac{d\Omega_{k'}}{4\pi}\frac{B^s_{k'\to 0}}{1+f\mu'^2} = P_L(k')\left[1+\frac{f}{3}+\frac{13}{21}\frac{\partial}{\partial \ln D_+} + \left(\frac{13}{7}+f\right)\frac{f}{3}\frac{\partial}{\partial f}-\frac{1+f\mu^2}{3}\frac{\partial}{\partial \ln k} - \frac{2f\mu^2}{3}(1-\mu^2)\frac{\partial}{\partial\mu^2}\right] \times D_+^2 P_{L0}(k)(1+f\mu^2)^2. \quad (66)$$

Collecting the various terms, we can check that we recover Eq. (65).

Therefore, we have checked the angular-averaged redshift-space consistency relation (41) for the bispectrum, at the leading order of perturbation theory, within the approximate symmetry $\Omega_m/f^2 \simeq 1$ discussed in Sec. III. In this explicit check, the use of this approximate symmetry appears at the level of the expression (58) of the bispectrum, which only involves the linear growing mode D_+ and the factor f as functions of time and cosmology. An exact calculation would give factors that show new but weak dependencies on time and cosmology [and that are unity for the Einstein–de Sitter (EdS) case] [4]. These deviations from Eq. (58) are usually neglected [for instance, when the cosmological constant is zero, they were shown to be well approximated by factors like $(\Omega_m^{-2/63}-1)$ that are very small over the range of interest [42]].

For future use in Sec. VII B 1 below, in terms of the angular monopole and quadrupole, Eq. (65) gives at the lowest order of perturbation theory

$$\int_{-1}^{1}\frac{d\mu}{2}\int\frac{d\Omega_{k'}}{4\pi}\frac{B^s_{k'\to 0}}{1+f\mu'^2} = P_L(k')\left\{(235+235f+101f^2+13f^3)\frac{P_L(k)}{105}-\frac{35+35f+21f^2+5f^3}{105}\frac{dP_L(k)}{d\ln k}\right\} \quad (67)$$

and

$$\frac{5}{2}\int_{-1}^{1}d\mu L_2(\mu)\int\frac{d\Omega_{k'}}{4\pi}\frac{B^s_{k'\to 0}}{1+f\mu'^2} = P_L(k')\left\{\frac{4f}{441}(420+303f+49f^2)P_L(k)-\frac{2f}{63}(21+18f+5f^2)\frac{dP_L(k)}{d\ln k}\right\}. \quad (68)$$

B. One-dimensional nonlinear check

The explicit check presented in Sec. VI A only applies up to the lowest order of perturbation theory. Because the goal of the consistency relations is precisely to go beyond low-order perturbation theory, it is useful to obtain a fully nonlinear check. This is possible in one dimension, where the Zel'dovich solution [43] becomes exact (before shell crossing) and all quantities can be explicitly computed. Because of the change of dimensionality, we also need to rederive the one-dimensional (1D) form of the consistency relations. We present the details of our computations in Appendix A and only give the main steps in this section.

In the 1D case, the redshift-space coordinate (5) now reads as

$$s = x+\frac{v}{\dot a} = x+fu, \quad (69)$$

where u is the rescaled peculiar velocity defined in Eq. (A4), in a fashion similar to Eq. (17), and the redshift-space density contrast (6) is now written as

$$k\neq 0:\ \tilde\delta^s(k,t) = \int\frac{dq}{2\pi}e^{-iks(q,t)}, \quad (70)$$

where we again discarded a Dirac term that does not contribute for $k\neq 0$ and q is the Lagrangian coordinate of the particles.

As in the 3D case, to derive the 1D consistency relations, we consider two universes with close cosmological parameters and expansion rates, $a'(t) = [1-\epsilon(t)]a(t)$. Again, from the "1D Friedmann equations," we find that $\epsilon(t) = \epsilon_0 D_+(t)$. Next, a uniform overdensity Δ_{L0} can be absorbed by a change of frame, with $\epsilon_0 = \Delta\delta_{L0}$. Then, to obtain the consistency relations, we need the impact of the large-scale overdensity Δ_{L0} on small-scale structures, which at lowest order is given by the dependence of the small-scale density contrast $\tilde\delta^s(k)$ on ϵ_0. As shown in Appendix A 2, this reads as

$$\frac{\partial\tilde\delta^s(k,t)}{\partial\epsilon_0} = D_+^2\frac{\partial\tilde\delta^s}{\partial D_+}+fD_+(1+f)\frac{\partial\tilde\delta^s}{\partial f} - (1+f)D_+k\frac{\partial\tilde\delta^s}{\partial k}. \quad (71)$$

As expected, this takes the same form as the 3D result (34), up to some changes of numerical coefficients. This leads to the equal-time redshift-space consistency relations (see Appendix A 3)

$$\left\langle \frac{\tilde{\delta}^s(k')}{1+f}\tilde{\delta}^s(k_1)\ldots\tilde{\delta}^s(k_n)\right\rangle'_{k'\to 0} = P_L(k')\left[1+f+\frac{\partial}{\partial \ln D_+}+(1+f)f\frac{\partial}{\partial f}-(1+f)\sum_{i=1}^{n}k_i\frac{\partial}{\partial k_i}\right]\langle\tilde{\delta}^s(k_1)\ldots\tilde{\delta}^s(k_n)\rangle'. \quad (72)$$

Here, we no longer need to average over the directions of the large-scale wave number k' because at equal times the leading-order contribution associated with the uniform displacement of small-scale structures by large-scale modes vanishes [17–23]. Indeed, because of statistical homogeneity and isotropy, equal-time polyspectra are invariant through uniform translations and cannot probe uniform displacements. Therefore, 1D equal-time statistics directly probe the next-to-leading order contribution (72), which truly measures the impact of large-scale modes on the growth of small-scale structures.

In the 1D case, the Zel'dovich approximation is exact until shell crossing [26,43], and it yields for the redshift-space nonlinear density contrast (70) the expression (see Appendix A 4)

$$\tilde{\delta}^s(k,t) = \int \frac{\mathrm{d}q}{2\pi} e^{-\mathrm{i}kq+k(1+f)D_+\int\frac{\mathrm{d}k'}{k'}e^{\mathrm{i}k'q}\tilde{\delta}_{L0}(k')}. \quad (73)$$

The expression (73) is exact at all orders of perturbation theory, but it no longer holds after shell crossing (which is a nonperturbative effect). On the other hand, we can define a 1D toy model by setting particle trajectories as equal to Eq. (A17). This system is no longer identified with a 1D gravitational system, and it only coincides with the latter in the perturbative regime, but it remains well defined and given by Eqs. (A17) and (73) in the nonperturbative shell-crossing regime.

Then, using the expression (73), we can explicitly check the 1D consistency relations (72). We present in Appendix A 5 two different checks. First, in Appendix A 5 a, we check Eq. (71) by explicitly computing the impact on the nonlinear density contrast (73) of a small change $\Delta\delta_{L0}$ to the initial conditions. Second, in Appendix A 5 b, we directly check the consistency relations (72) by explicitly computing the correlations $\langle\tilde{\delta}_L(k')\tilde{\delta}^s(k_1)\ldots\tilde{\delta}^s(k_n)\rangle'_{k'\to 0}$ and $\langle\tilde{\delta}^s(k_1)\ldots\tilde{\delta}^s(k_n)\rangle'$ and verifying that they satisfy Eq. (72).

These two different checks allow us to check both the reasoning that leads to the consistency relations, through the intermediate result (71), and the final expression of these relations. They also explicitly show that they are not restricted to the perturbative regime. In particular, they extend beyond shell crossing, as seen from the toy model defined by the explicit expression (73) (i.e., where one defines the system by the Zel'dovich dynamics, even beyond shell crossing, without further reference to gravity).

As for the real-space consistency relations [26], it happens that in this 1D model (73) the 1D consistency relations (72) are actually exact, that is, they do not rely on the approximation $\kappa \simeq \kappa_0$, where κ defined in Eq. (A8) plays the role of the 3D factor Ω_m/f^2 encountered in Eqs. (19)–(21). This is because the redshift-space density contrast (73) truly only depends on cosmology and time through the two factors D_+ and f, even at the nonlinear order. In contrast, in the 3D gravitational case, beyond linear order, new functions of cosmology and time appear (for cosmologies that depart from the Einstein–de Sitter case), and they can only be reduced to powers of D_+ and f within the approximation $\Omega_\mathrm{m}/f^2 \simeq 1$. On the other hand, if we consider the actual 1D gravitational dynamics even beyond shell crossing, where it deviates from the expression (73), then the 1D consistency relations (72) are only approximate in the nonperturbative regime, as they rely on the approximation $\kappa \simeq \kappa_0$, while remaining exact at all perturbative orders.

Unfortunately, it is not easy to build 3D analytical models that can be explicitly solved and suit our purposes. The 3D Zel'dovich approximation again provides a simple model for the formation of large-scale structures and the cosmic web. However, it cannot suit our purposes because it does not apply to the dynamics of the 3D background universe itself. Indeed, as can be seen from their derivation in Sec. IV, the consistency relations precisely derive from the fact that a large-scale almost uniform density perturbation can be seen as a local change of the cosmological parameters (i.e., the background density). This is also apparent through the fact that the deviation $\epsilon(t)$ between the two nearby universes (23) obeys the same evolution equation (16) as the linear growing mode of local density perturbations. This is no longer possible for the 3D Zel'dovich approximation, which is not an exact solution and cannot be extended to the Hubble flow itself. In contrast, in the 1D universe, the Zel'dovich approximation is actually exact (before shell crossing), and it applies both at the level of the background and of the density perturbations. An alternative dynamics, which is exact at the background level and provides analytical results on small nonlinear scales, is the spherical collapse model. However, this yields a very different density field than the actual one, as there is a single central density fluctuation that breaks statistical homogeneity and density correlations are no longer invariant through translations. Therefore, although it should be possible to obtain some consistency relations for this model, they would have a rather different form, and this 1D spherical model would be even farther from the actual universe than the 1D statistically homogeneous model studied in this section.

VII. SIMULATIONS

The angular-averaged consistency relations (37)–(41) are valid at all orders of perturbation theory and also beyond

the perturbative regime, including shell-crossing effects, within the accuracy of the approximation $\Omega_{\rm m}/f^2 \simeq 1$ (and as long as gravity is the dominant process). We have explicitly confirmed them either perturbatively or nonperturbatively, but the latter is limited to the one-dimensional case.

It would thus be of great importance to further check these relations in three dimensions nonperturbatively. We exploit here a series of N-body simulations for this purpose. As can be seen in the following, they are also useful to understand the possible breakdown of the relations and test the validity of the *ansatz* employed in the measurement in practical situations. We first summarize how we can evaluate the derivative terms in the consistency relations. We then present the numerical results for the bispectrum together with a brief description of the simulations themselves.

A. Derivatives from numerical simulations

The consistency relation (43) involves derivatives with respect to D_+ and f. They can be obtained at once within the framework of an explicit analytic model for the matter density polyspectra. However, in this paper, we do not use these relations to check a specific analytical model. Instead, we wish to use numerical simulations to test these relations (which are only approximate because of the approximation $\Omega_{\rm m}/f^2 \simeq 1$). Nevertheless, we can also measure separately the derivatives with respect to D_+ and f from the simulations.

The redshift-space coordinate $\boldsymbol{s}$ can be written in terms of the comoving coordinate $\boldsymbol{x}$ and peculiar velocity $\boldsymbol{v}$ as in Eq. (30). As explained in Sec. III, within the approximation $\Omega_{\rm m}/f^2 \simeq 1$ that is used to derive the consistency relations, all time dependence can be absorbed in the linear growing mode $D_+(t)$ with the change of variables (17). This means that the fields $\{\delta, \mathbf{u}, \varphi\}$ are only functions of time through D_+, as well as the displacement field $\Psi(\mathbf{q}, t) = \boldsymbol{x} - \mathbf{q}$, where $\mathbf{q}$ is the Lagrangian coordinate of the particles. Thus, for a given realization defined by the linear density field $\delta_{L0}(\mathbf{q})$ (normalized today or at the initial time of the simulation), the redshift-space coordinate $\boldsymbol{s}$ depends on the functions $D_+(t)$ and $f(t)$ as

$$\boldsymbol{s}(\mathbf{q}, t) = \boldsymbol{x}(\mathbf{q}, D_+) + f u_r(\mathbf{q}, D_+)\mathbf{e}_r. \tag{74}$$

Therefore, a small change Δf of the factor f corresponds to a change of the redshift-space coordinate $\boldsymbol{s}(\mathbf{q})$ of the particles given by

$$f \to f + \Delta f\colon \boldsymbol{s} \to \boldsymbol{s} + \Delta f u_r \mathbf{e}_r = \boldsymbol{s} + \Delta f \frac{v_r}{\dot{a} f}\mathbf{e}_r. \tag{75}$$

On the other hand, from the equations of motion (19)–(21), a change $\Delta \ln D_+$ of the linear growing mode leads to a change of the particle velocities and coordinates,

$$\ln D_+ \to \ln D_+ + \Delta \ln D_+\colon \boldsymbol{x} \to \boldsymbol{x} + \Delta \ln D_+ \mathbf{u},$$
$$\mathbf{u} \to \mathbf{u} - \Delta \ln D_+ \left[\left(\frac{3\Omega_{\rm m}}{2f^2} - 1\right)\mathbf{u} + \nabla\varphi\right], \tag{76}$$

whence

$$\boldsymbol{s} \to \boldsymbol{s} + \Delta \ln D_+ \left[\mathbf{u} - f\left(\left(\frac{3\Omega_{\rm m}}{2f^2} - 1\right)u_r + \frac{\partial\varphi}{\partial r}\right)\mathbf{e}_r\right]$$
$$= \boldsymbol{s} + \Delta \ln D_+ \left[\frac{\boldsymbol{v}}{\dot{a} f} - \left(\left(\frac{3\Omega_{\rm m}}{2f^2} - 1\right)\frac{v_r}{\dot{a}} + \frac{1}{\dot{a}^2 f}\frac{\partial\phi}{\partial r}\right)\mathbf{e}_r\right]. \tag{77}$$

Thus, to obtain the partial derivative of the power spectrum with respect to f or $\ln D_+$, we modify the particle redshift-space coordinates by Eqs. (75) or (77), for a small value of Δf or $\Delta \ln D_+$, and we compute the associated power spectrum. Taking the difference from the initial power spectrum and dividing by Δf or $\Delta \ln D_+$ gives a numerical estimate of $\partial P^s/\partial f$ or $\partial P^s/\partial \ln D_+$.

B. Numerical results

We are now in a position to present the consistency relations measured from simulations. Before that, let us briefly describe the simulations used here. They are the ones performed in Ref. [9]. Employing 1024^3 dark matter particles in a periodic cube of $(2048\ h^{-1}{\rm Mpc})^3$, the gravitational dynamics was solved by the public simulation code `Gadget2` [44] starting from an initial condition set at $z = 15$ by solving second-order Lagrangian perturbation theory [39,45,46]. The cosmological model used was a flat-ΛCDM model consistent with the five-year observation of the WMAP satellite [47]: $\Omega_{\rm m} = 0.279$, $\Omega_{\rm b} = 0.165\Omega_{\rm m}$, $h = 0.701$, $A_{\rm s} = 2.49 \times 10^{-9}$, and $n_{\rm s} = 0.96$ at $k_0 = 0.002\,{\rm Mpc}^{-1}$. This whole process was repeated 60 times with the initial random phases varied to have a large ensemble of random realizations.

The consistency relations have already been examined and presented in real space in Ref. [28]. There, it was found that the relation was consistent with the N-body simulations within their statistical uncertainty at $z = 1$, while a discrepancy of the several percent level was found at $z = 0.35$. It was further discussed that this is presumably due to the breakdown of the approximation $\Omega_{\rm m}/f^2 \simeq 1$; for instance, we found that the relations better hold in supplementary simulations done in the EdS background, but with exactly the same initial perturbations. We focus here on the lower redshift, $z = 0.35$, at which the consistency relations are the most nontrivial.

1. Full consistency relations

We first consider the redshift-space consistency relations in their full form (48)–(49), with both derivative operators $\partial/\partial D_+$ and $\partial/\partial f$.

Having already presented the methods we employ to measure the derivative terms in the previous subsection, the postprocessing for the simulation outputs is exactly the same as in Ref. [28] except that we now consider the particle positions in redshift space. The matter density field is constructed with the Cloud-in-Cells (CIC) interpolation on 1024^3 mesh cells, and subsequent computations are based on the fast Fourier transform. The change in the particle coordinates corresponding to a slight change in $\ln D_+$ is also computed based on the calculation on the same mesh cells for $\partial\phi/\partial r$ and then interpolated to the positions of particles using the CIC kernel [see Eq. (77)].

The monopole and the quadrupole moments of the relation for the bispectra, Eqs. (48) and (49), are, respectively, shown in the left and the right panels of Fig. 1. In each panel, we fix the value of the larger wave number k and plot the ratio of the two sides as a function of the smaller wave number k'. The error bars are estimated based on the scatter among the 60 independent realizations. They thus correspond to the error level expected for an ideal survey with a volume of $\sim 8\ h^{-3}\mathrm{Gpc}^3$ when we can ignore the shot-noise contamination. Overall, the ratio is close to unity for both the monopole and quadrupole. From this figure, we basically confirm the relations at the nonperturbative level in the three-dimensional dynamics.

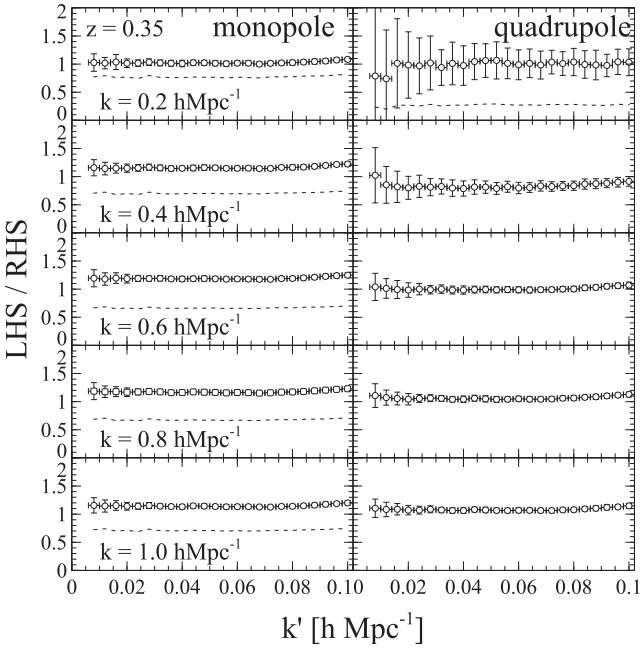

FIG. 1. Consistency-relation ratio for the redshift-space bispectrum from N-body simulations. The circles with error bars show our numerical measurements, while the dashed lines show the ratio of the measured bispectrum to its tree-order predictions (67) and (68). We omit the statistical errors on the dashed lines for clarity, but they are very similar to those on the circles. Note that the dashed lines fall out of the plotted range for the quadrupole moment on small scales ($k \geq 0.4\,h\mathrm{Mpc}^{-1}$), as they take the wrong sign.

The dashed lines in Fig. 1 show the ratio of the measured bispectrum to its tree-order predictions (67) and (68). For the monopole, this lowest-order perturbative prediction fares reasonably well as it only underestimates the nonlinear results by 30%, on these scales. However, it is already less accurate than our result (48), which takes into account higher-order and nonperturbative nonlinear corrections (at the price of the approximation $\Omega_\mathrm{m}/f^2 \simeq 1$). For the quadrupole, the lowest-order perturbative prediction does not appear in the panels at $k \geq 0.4\,h\mathrm{Mpc}^{-1}$ because in these cases it is out of range and actually gives the wrong sign. This change of sign is likely due to the fingers-of-god (FOG) effect, which is not captured by perturbation theory. Indeed, it is well known that higher-order multipoles are increasingly sensitive to small-scale nonlinear contributions, as FOG effects impart a strong angular dependence to the bispectrum [32].

We can confirm this from Fig. 2; we remove most of the FOG effect from the simulated density field in redshift space by relocating all the member particles of friends-of-friends halos to the centers of mass. We do this to one of our 60 realizations and measure the same angular-averaged bispectra (symbols), which are compared with the original measurement (solid lines) from the same realization. The difference between the symbols and the lines is more prominent for higher multipoles and on smaller scales. The

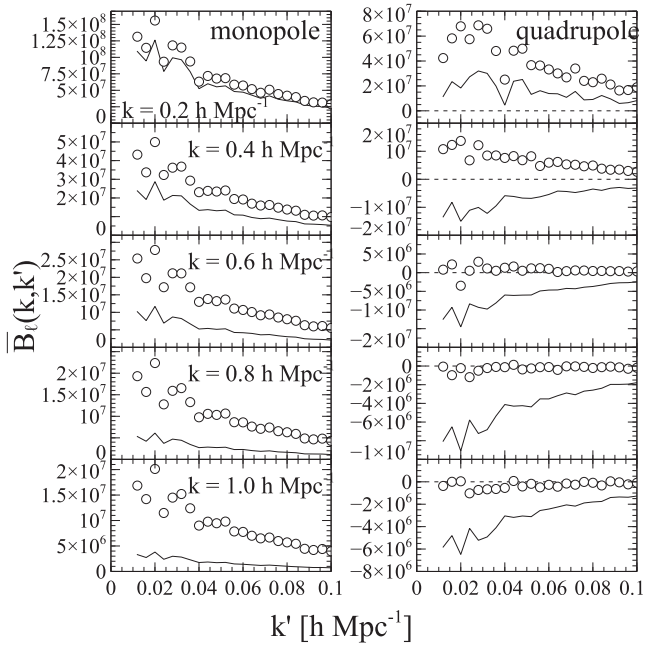

FIG. 2. Impact of the finger-of-god effect on the angular-averaged bispectra. We show by the symbols the multipole moments of the bispectra after the FOG removal with the procedure explained in the text. The original measurement without this compression is shown by the solid line. Note that this exercise is done with one of our 60 realizations, and the result from the same realization is shown for the original measurement for a fair comparison.

monopole moment differs by as much as a factor 5 at $k = 1\ h\mathrm{Mpc}^{-1}$ before and after the FOG removal, highlighting the importance of the FOG effect. The quadrupole moment has a different sign in the two measurements at $k = 0.4\ h\mathrm{Mpc}^{-1}$, and the negative bispectrum on the smaller scale is mostly damped when FOG is compressed by hand.

In contrast to the perturbative calculation, our result (49) remains consistent with the simulation data within 20% in Fig. 1. This shows that we test the consistency relations in a nontrivial regime, beyond the reach of standard perturbation theory. Thus, the tradeoff between the error introduced by the approximate symmetry of Sec. III and the advantage of taking into account all nonlinear contributions, at both perturbative and nonperturbative levels, is beneficial. This is particularly true for complex statistics such as the redshift-space quadrupole that are very sensitive to small-scale highly nonlinear effects, which are difficult to include in analytical modelings.

However, when we look into each panel more closely, we can find that the data points are slightly off from unity. For the monopole moment, the ratio tends to be larger than unity at $k \gtrsim 0.4\ h\mathrm{Mpc}^{-1}$. On the other hand, unity is within the statistical error level for the quadrupole moment, though the central values are larger (smaller) than unity on $k \lesssim 0.4\ h\mathrm{Mpc}^{-1}$ ($k \gtrsim 0.8\ h\mathrm{Mpc}^{-1}$). In most of the cases, the deviation from unity is at most 20%, and this is meaningful only when we measure the ratio very precisely; an ideal survey with a volume of $\sim 8\ h^{-3}\mathrm{Gpc}^3$ can detect the deviation from unity only for the monopole moment on small scales.

These deviations are somewhat greater than those found in Ref. [28] in real space, which only reached 7% at $k = 1\ h\mathrm{Mpc}^{-1}$. This is not surprising because it is well known that redshift-space statistics are more sensitive to small nonlinear scales, for instance, through the fingers-of-god effect, and low-order perturbation theory has a smaller range of validity. Then, we can expect a greater violation of the redshift-space consistency relations because the breakdown of the approximation $\Omega_\mathrm{m}/f^2 \simeq 1$ has a stronger impact on higher perturbative orders. Indeed, absorbing the time and cosmological dependence by $D_+(t)$ and $f(t)$ is exact at linear order, whereas higher orders involve new functions $D_+^{(n)}(t)$ that are not exactly equal to $D_+(t)^n$ [4], and the discrepancies may cumulate in the nonlinear regime.

We then work on the supplemental simulations done in the EdS background to understand the cause of this small discrepancy, just as in our previous real-space paper [28]. Note that our consistency relations in an Einstein–de Sitter cosmology also involve the approximate symmetry described in Sec. III, even though $\Omega_\mathrm{m}/f^2 = 1$ in the EdS background. Indeed, what matters is not that Ω_m/f^2 is unity in the reference cosmology but that Ω_m/f^2 remain (approximately) constant as we vary the background curvature around the reference cosmology. Nevertheless, the comparison between EdS and ΛCDM results provides a simple estimate of the impact of our approximation because the difference between these two cosmologies arises from the change of the reference point along the Ω_m/f^2 curve.

The results from four realizations of such simulations are shown in Fig. 3. Although the scatter of the data points is larger than in Fig. 1, the systematic departure from unity in the previous figure is clearly reduced. We thus conclude that the small violation of the consistency relations for the bispectrum can be explained by the breakdown of the approximation $\Omega_\mathrm{m}/f^2 \simeq 1$ (more precisely, of constant Ω_m/f^2 for nearby background curvatures), in agreement with the discussions above.

2. $f\mu^2$ ansatz and reduction to $\partial/\partial D_+$ operator

Now, we come back to the original ΛCDM simulations and apply the *ansatz* that all the f and μ dependences appear through the combination $f\mu^2$. This allows us to replace the f derivatives, $\partial/\partial f$, by μ^2 derivatives, $\partial/\partial\mu^2$, as in Eq. (50). This gives the approximated consistency relations for the bispectrum, Eqs. (54) and (55), respectively, for the monopole and quadrupole moment, which we plot in Fig. 4. In contrast with the exact form of the consistency relations, given by Eqs. (48) and (49) and displayed in Fig. 1, the right-hand side now involves an infinite summation over all Legendre multipoles of the

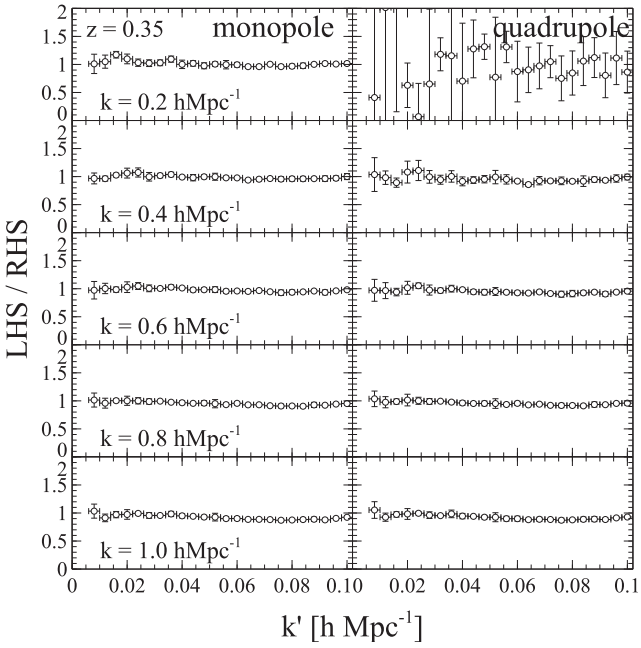

FIG. 3. Same as Fig. 1, but for the simulations performed in EdS background expansion. Note that we have only four realizations for the EdS simulation, and this is the reason why we have a larger statistical error than in Fig. 1.

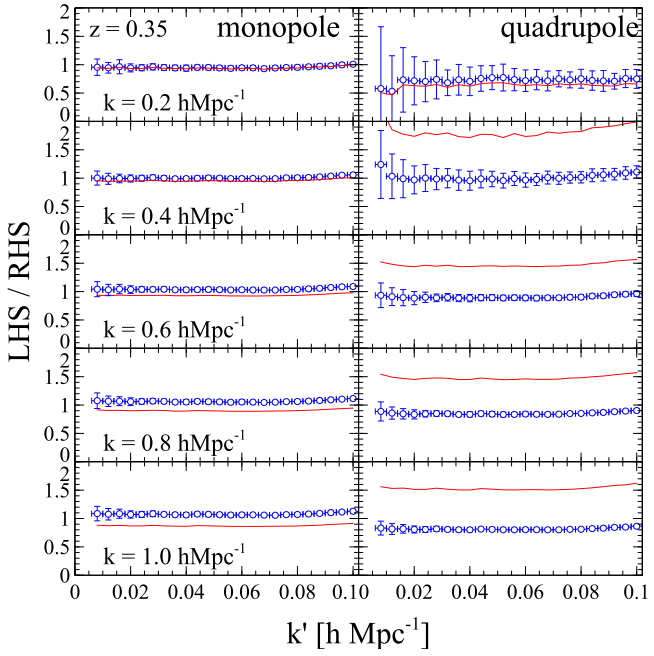

FIG. 4 (color online). Same as Fig. 1, but for Eqs. (54) and (55) after applying the *ansatz* to rewrite the f-derivative terms. The circles and the solid lines, respectively, show the ratio truncated at P_2^s and P_4^s.

redshift-space power spectrum. Here, we truncate these series at order P_2^s (circles) or P_4^s (solid lines).

The difference between the symbols and the lines is negligible at $k = 0.2$ and $0.4\ h\mathrm{Mpc}^{-1}$ for the monopole and $k = 0.2\ h\mathrm{Mpc}^{-1}$ for the quadrupole moment, where the ratio itself is roughly consistent with unity. As we move to smaller scales, the symbols and the lines become more distinct. In those cases, adding the higher-order term (i.e., P_4^s) does not help to restore the relations, suggesting that the *ansatz* is not a good approximation at the corresponding scales. The plot suggests that the quadrupole moment is more sensitive to the higher-order term and thus the *ansatz* works less accurately than for the monopole moment. This is naturally expected since the quadrupole moment is impacted more strongly by higher-order corrections (see, e.g., Ref. [48], where we can see how much higher-order perturbative corrections affect the first two moments; these corrections have terms $\mu^{2m} f^n$, where m and n can be different).

3. $f\mu^2$ ansatz and further reduction to $\partial/\partial a$ operator

The situation is basically the same after we further apply the *ansatz* to replace the derivative with respect to D_+ by a derivative with respect to time or the scale factor, as in Eq. (52). As compared with the form displayed in Fig. 4, this involves an additional approximation, which relies on the same $f\mu^2$ *ansatz* because the full time derivative, or scale-factor derivative, $\partial/\partial a$, combines both theoretical derivatives $\partial/\partial D_+$ and $\partial/\partial f$. Therefore, to replace the operator $\partial/\partial D_+$ by $\partial/\partial a$, we must once again use the $f\mu^2$ *ansatz* to remove the new $\partial/\partial f$ terms generated by the change of variable from D_+ to a.

Figure 5 shows the results of Eqs. (56) and (57). The solid lines for the truncation at the P_4^s order are now out of the plotted range for the quadrupole moment on small scales. The relation for the monopole moment is more robust against this approximation *ansatz* on large scales, especially at $k = 0.2\ h\mathrm{Mpc}^{-1}$, and we can safely apply the consistency relation here in the simplified form (56). Except for this case, the ratio is affected significantly by the *ansatz* and the order at which we truncate the infinite summation on the right-hand side. Nevertheless, we note that by truncating at order P_2^s we obtain a good agreement, better than 20% up to $k = 1\ h\mathrm{Mpc}^{-1}$, for the monopole. For the quadrupole, the deviation can reach up to 40%.

Therefore, even with the current *ansatz*, we can still examine how the ratio behaves in the observations and compare it with the simulation results. Since the data points obtained with the truncation at order P_2^s (i.e., circles) are less noisy and moreover stay around unity after applying the *ansatz*, the easiest check of the true gravitational dynamics is to apply the same *ansatz* and truncate the moments at this order. We would need a more involved *ansatz* for the estimation of the derivative terms from observations to extend the applicable range of these consistency relations, and we leave this to a future study.

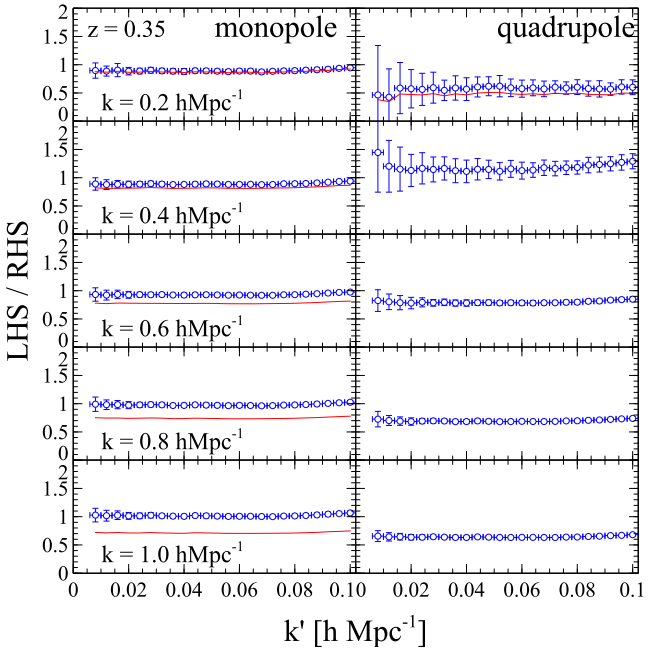

FIG. 5 (color online). Same as Fig. 4, but for Eqs. (56) and (57) after applying the *ansatz* once again to convert the D_+-derivative terms into the a derivatives. Note that the lines for the quadrupole moment fall below (above) the plotted range at $k = 0.4$ (0.6, 0.8 and 1.0) $h\mathrm{Mpc}^{-1}$.

VIII. SUMMARY

In this paper, we have generalized the equal-time angular-averaged consistency relations for the cosmic density field originally developed in real space by Ref. [26] to redshift space, in which the actual observations are taking place. These relations express the squeezed limit of $(n+1)$-point correlation functions or polyspectra, with n small-scale modes (that can be in the nonlinear regime) and one large-scale mode (in the linear regime at a much larger scale than all other n wave numbers), in terms of the n-point correlation of the small-scale modes. These relations can be generalized to $(n+\ell)$ correlations, with ℓ large-scale modes, as in Ref. [26], but we focused here on the case of one large-scale mode. The explicit forms that we have obtained rely on an approximate symmetry of the dynamics, $\Omega_{\rm m}/f^2 \simeq 1$. However, within this approximation, they are valid at a fully nonlinear level. Thus, they hold at all orders of perturbation theory and also in the nonperturbative regime, beyond shell crossing. In particular, they include both the large-scale Kaiser effect [35], associated with the infall of matter within large-scale gravitational wells, and the fingers-of-god effect [34], associated with the virial motions inside collapsed halos.

We have found that, because the mapping from the real to redshift space involves the velocity component along the radial direction, the form of these consistency relations is slightly more complex than in real space, as it involves two types of time derivatives. The first is a derivative with respect to the linear growing mode $D_+(t)$, which also appeared in the real-space case. The second is a derivative with respect to the linear growth rate, $f(t) = {\rm d}\ln D_+/{\rm d}\ln a$. This differential operator, $\partial/\partial f$, did not appear in the real-space case, and it arises from the scaling of the peculiar velocity field (i.e., through the change of variable from $\boldsymbol{v}$ to $\mathbf{u}$, where $\mathbf{u}$ is the rescaled velocity field that makes use of the approximate symmetry of the dynamics). This feature makes it more difficult to use these relations for observations because at best we can only measure one time derivative, $\partial/\partial t$, which combines both $\partial/\partial D_+$ and $\partial/\partial f$, and we cannot measure these two derivatives separately. However, these relations can still be used to check analytical models or numerical simulations, where we can explicitly compute these two derivatives.

Next, we have tested these consistency relations both analytically and numerically. First, at the leading order of perturbation theory, we have checked the lowest-order consistency relation, which expresses the squeezed limit of the bispectrum in terms of the nonlinear power spectrum of the small-scale modes. Second, in a fully nonlinear and nonperturbative analysis, we have checked all these consistency relations at all orders, in the simpler one-dimensional case, where we can use the exact Zel'dovich solution of the dynamics.

We have also tested the lowest-order consistency relations, relating the nonlinear bispectrum and power spectrum, with numerical simulations. We find a reasonably good agreement at $z = 0.35$. Projecting the angular dependence of the redshift-space polyspectra onto Legendre polynomials, we find a good agreement for the monopole up to $k \lesssim 0.4\,h{\rm Mpc}^{-1}$, and we detect a small deviation of at most 20% for $k \leq 1\,h{\rm Mpc}^{-1}$. For the quadrupole, we do not detect significant deviations (but the statistical error bars are slightly larger). In the case of an Einstein–de Sitter cosmology, we find that these deviations are greatly reduced and our numerical data agree with theoretical predictions. Therefore, the small deviations found in the ΛCDM cosmology can be explained by the finite accuracy of the approximation $\Omega_{\rm m}/f^2 \simeq 1$.

The typical magnitude of these deviations is larger and extends over a wider wave number range than for the real-space consistency relations [28]. This is consistent with the observation that the nonlinearity in the cosmic velocity field is more sensitive to the local nonlinear structure on small scales, as small-scale effects can easily propagate to larger scales through the nonlinear mapping from the real to the redshift space. Indeed, it is well known that the perturbation-theory prediction of the matter power spectrum is more difficult in redshift space [4]. Then, because nonlinear effects are likely to amplify the breakdown of the approximation $\Omega_{\rm m}/f^2 \simeq 1$, violations of the consistency relations due to the breakdown of this approximate symmetry are indeed expected to be greater in redshift space.

On the other hand, we find that our results for the bispectrum provide a significant improvement over lowest-order perturbation theory, especially for the quadrupole where the perturbative prediction even gives the wrong sign for $k \geq 0.4\,h{\rm Mpc}^{-1}$. This is a signature of the strong impact of small-scale nonlinearities onto redshift-space statistics, which is usually difficult to model analytically. In particular, by comparing our results with density fields where the fingers-of-god effect is removed by replacing particles by their host halo, we find that we can probe scales where the fingers-of-god effects are important and can even change the sign of the quadrupole. This shows that we test the consistency relations in a nontrivial regime, beyond low-order perturbation theory. It also shows the interest of these nonlinear relations, as the inaccuracy introduced by the approximate symmetry $\Omega_{\rm m}/f^2 \simeq 1$ is more than compensated by the account of higher-order and nonperturbative nonlinear contributions. This can be even more beneficial for statistics such as the redshift-space quadrupole that are sensitive to highly nonlinear effects that are difficult to model.

To make the connection with observations, or to simplify the form of these consistency relations, we also tested a simple *ansatz* that allows one to remove the new operator $\partial/\partial f$. This relies on the approximation that f and μ^2 only enter the redshift-space power spectrum through the combination $f\mu^2$ (this is exact at linear order, in the Kaiser effect). A first step allows us to remove the operator $\partial/\partial f$,

which only leaves the operators $\partial/\partial D_+$ and $\partial/\partial k$ in multipole space. The drawback is that the right-hand side of each consistency relation now involves an infinite series over multipoles of all orders. We find that this approximation gives rise to an additional source of discrepancy between the numerical data and the analytic predictions, especially for the quadrupole. Moreover, the result depends on the order at which we truncate the multipole series in the right-hand side. It turns out that better results are obtained when we truncate at the lowest-order P_2^s. This suggests that the $f\mu^2$ *ansatz* does not faithfully describe higher perturbative or nonperturbative orders.

In a second step, we use once more the $f\mu^2$ *ansatz* to replace the operator $\partial/\partial D_+$ by the full time derivative, or scale-factor derivative $\partial/\partial a$. As could be expected, we find that this further increases the deviation from the numerical simulation data and the dependence on the truncation order, especially for the quadrupole.

Nevertheless, we find that using the $f\mu^2$ *ansatz* and truncating at order P_2^s we obtain an agreement that is better than 20% up to $k = 1\,h\mathrm{Mpc}^{-1}$ for the monopole. For the quadrupole, the deviation can reach 40%. Although these limitations make the accessible range of these consistency relations rather narrow, we can still make use of them to predict the higher-order polyspectra. There is substantial recent progress on the redshift-space clustering, but the calculations are mostly limited to the power spectrum (e.g., Refs. [33,48–52]). Using the relations developed here, one can compute, for instance, the angular-averaged bispectrum in redshift space by substituting these formulas for the power spectrum. Since the relations approximately hold down to very small scales, albeit not perfectly, they can be useful in estimating the covariance matrices of the redshift-space observables (we need the trispectrum to compute the matrix for the power spectrum). Indeed, the accuracy required for the covariance matrices might not be as demanding as that for the spectra themselves. A study along this line is undergoing now, and we wish to present the results elsewhere in the near future.

A more complex issue is the problem of biasing, when we wish to connect measures from galaxy surveys with theoretical predictions. In principle, the approximate symmetry $\Omega_\mathrm{m}/f^2 \simeq 1$ that we used to obtain explicit expressions no longer applies once we take into account galaxy formation physics. Indeed, baryonic processes (cooling, star formation, etc.) involve new characteristic scales that explicitly break the symmetry of the dynamics. Then, *a priori* it is no longer possible to absorb the time dependence of the dynamics by a simple rescaling that only involves the linear growing mode. Therefore, the relations we have obtained are not guaranteed to apply to the galaxy density field itself, by making the naive replacement $\delta \to \delta_\mathrm{g}$. One should rather use these relations as constraints on the matter density field and, given a supplementary model that relates the galaxy field to the dark matter density field, derives the consequences onto the galaxy density field. Of course, this would depend on the model that is used to describe galaxy formation and introduce an additional approximation. We leave such a study for future works.

ACKNOWLEDGMENTS

This work is supported in part by the French Agence Nationale de la Recherche under Grant No. ANR-12-BS05-0002. T. N. is supported by Japan Society for the Promotion of Science Postdoctoral Fellowships for Research Abroad. The numerical calculations in this work were carried out on Cray XC30 at Center for Computational Astrophysics of National Astronomical Observatory of Japan.

APPENDIX A: 1D EXAMPLE

As for the real-space consistency relations [26], it is interesting to check the redshift-space consistency relations (37)–(41) obtained in this paper by using a simple one-dimensional example that can be exactly solved. This is again provided by the Zel'dovich dynamics [43], which is exact in one dimension (before shell crossing).

1. 1D equations of motion

The 1D version of Eqs. (13)–(15) reads as [26]

$$\frac{\partial\delta}{\partial t} + \frac{1}{a}\frac{\partial}{\partial x}[(1+\delta)v] = 0, \tag{A1}$$

$$\frac{\partial v}{\partial t} + Hv + \frac{1}{a}v\frac{\partial v}{\partial x} = -\frac{1}{a}\frac{\partial\phi}{\partial x}, \tag{A2}$$

$$\frac{\partial^2\phi}{\partial x^2} = 4\pi\mathcal{G}(t)\bar{\rho}a^2\delta. \tag{A3}$$

Here, we generalized the 1D gravitational dynamics to the case of a time-dependent Newton's constant $\mathcal{G}(t)$. This allows us to obtain ever-expanding cosmologies, similar to the 3D Einstein–de Sitter cosmology, for power-law cases $\mathcal{G}(t) \propto t^\alpha$ with $-2 < \alpha < -1$ [and $a(t) \propto t^{\alpha+2}$, $\bar{\rho}(t) \propto 1/a(t) \propto t^{-(\alpha+2)}$].

Linearizing these equations, we obtain the evolution equation of the linear modes of the density contrast. It takes the same form as the usual 3D equation (16), $\ddot{D} + 2H(t)\dot{D} - 4\pi\mathcal{G}(t)\bar{\rho}(t)D = 0$, but with a time-dependent Newton's constant and the 1D scale factor $a(t)$.

In a fashion similar to the change of variables (17), we make the change of variables

$$\eta = \ln D_+, \qquad v = \dot{a}fu, \qquad \phi = (\dot{a}f)^2\varphi, \quad \text{with}$$
$$f = \frac{a\dot{D}_+}{\dot{a}D_+}, \tag{A4}$$

and we obtain the rescaled equations of motion

$$\frac{\partial\delta}{\partial\eta}+\frac{\partial}{\partial x}[(1+\delta)u]=0, \tag{A5}$$

$$\frac{\partial u}{\partial\eta}+[\kappa(t)-1]u+u\frac{\partial u}{\partial x}=-\frac{\partial\varphi}{\partial x}, \tag{A6}$$

$$\frac{\partial^2\varphi}{\partial x^2}=\kappa(t)\delta, \tag{A7}$$

where we introduced the factor $\kappa(t)$ defined by

$$\kappa(t)=4\pi\mathcal{G}(t)\bar{\rho}(t)\frac{D_+(t)^2}{\dot{D}_+(t)^2}. \tag{A8}$$

Thus, $\kappa(t)$ plays the role of the ratio $3\Omega_{\rm m}/(2f^2)$ encountered in the 3D case in Eqs. (19)–(21). Then, the 3D approximation $\Omega_{\rm m}/f^2\simeq 1$ used in the main text corresponds in our 1D toy model to the approximation $\kappa\simeq\kappa_0$. That is, we neglect the dependence of κ on the cosmological parameters and time, and the dependence on the background is fully contained in the change of variables (A4). [The generalization to the case of a time-dependent Newton's constant is not important at a formal level because it does not modify the form of the equations of motion. However, it is necessary for this approximate symmetry to make practical sense so that we can find a regime where κ is approximately constant. This corresponds to cosmologies close to the Einstein–de Sitter-like expansion $a(t)\propto t^{\alpha+2}$, in the case $\mathcal{G}(t)\propto t^{\alpha}$ with $-2<\alpha<-1$.]

The fluid equations (A5)–(A7) only apply to the single-stream regime, but we can again go beyond shell crossings by using the equation of motion of trajectories, which reads as

$$\frac{\partial^2 x}{\partial\eta^2}+[\kappa(t)-1]\frac{\partial x}{\partial\eta}=-\frac{\partial\varphi}{\partial x}, \tag{A9}$$

where φ is the rescaled gravitational potential (A7). This is the 1D version of Eq. (22), and it explicitly shows that particle trajectories obey the same approximate symmetry, before and after shell crossings.

2. 1D background density perturbation

To derive the 1D consistency relations, we follow the method described in the main text for the 3D case; see also the Appendix in Ref. [26]. As in Eq. (23), we consider two universes with close cosmological parameters, $a'(t)=a(t)[1-\epsilon(t)]$ and $\bar{\rho}'(t)=\bar{\rho}(t)[1+\epsilon(t)]$. Substituting into the 1D Friedmann equation, we again find that $\epsilon(t)$ obeys the same equation as the 1D linear growing mode $D_+(t)$, and we can write $\epsilon(t)=\epsilon_0 D_+(t)$.

Next, the change of frame described in Eq. (26) becomes

$$x'=(1+\epsilon)x,\qquad \delta'=\delta-\epsilon(1+\delta),\qquad v'=v+\dot{\epsilon}ax, \tag{A10}$$

and at linear order over both δ and ϵ, we have $\delta_L=\delta'_L+\epsilon$. This means that the background density perturbation ϵ is again absorbed by the change of frame, with $\epsilon_0=\Delta\delta_{L0}$. The redshift-space coordinate s now transforms as

$$s'=\left(1+\epsilon+\frac{\dot{\epsilon}}{H}\right)s. \tag{A11}$$

Then, as in Eq. (29), the redshift-space density contrast in the actual unprimed frame, with the uniform overdensity $\Delta\delta_{L0}$, is written as

$$k\neq 0:\ \tilde{\delta}^s_{\epsilon_0}(k,t)=\tilde{\delta}^s[(1-\epsilon-\dot{\epsilon}/H)k,D_{+\epsilon_0},f_{\epsilon_0}], \tag{A12}$$

where we disregarded the Dirac factor that does not contribute for wave numbers $k\neq 0$. Therefore, the derivative of the redshift-space density contrast with respect to ϵ_0 reads as

$$\frac{\partial\tilde{\delta}^s(k,t)}{\partial\epsilon_0}=\frac{\partial D_{+\epsilon_0}}{\partial\epsilon_0}\frac{\partial\tilde{\delta}^s}{\partial D_+}+\frac{\partial f_{\epsilon_0}}{\partial\epsilon_0}\frac{\partial\tilde{\delta}^s}{\partial f}-(1+f)D_+k\frac{\partial\tilde{\delta}^s}{\partial k}. \tag{A13}$$

As shown in Ref. [26], the derivative of the linear growing mode is $\partial D_+/\partial\epsilon_0=D_+^2$, which means that $D'_+=D_++\epsilon_0 D_+^2$. Then, using $a'=a-\epsilon_0 D_+ a$ and the definition (A4) for f and f', we obtain $f'=f+f(\epsilon+\dot{\epsilon}/H)$, whence

$$\left.\frac{\partial D_{+\epsilon_0}}{\partial\epsilon_0}\right|_{\epsilon_0=0}=D_+^2,\qquad \left.\frac{\partial f_{\epsilon_0}}{\partial\epsilon_0}\right|_{\epsilon_0=0}=fD_+(1+f). \tag{A14}$$

Therefore, Eq. (A13) gives Eq. (71).

3. 1D consistency relations

Using the result (71), the 1D version of the consistency relations (37) is written as

$$\begin{aligned}&\frac{1}{2}\sum_{\pm k'}\langle\tilde{\delta}_{L0}(k')\tilde{\delta}^s(k_1,t_1)\ldots\tilde{\delta}^s(k_n,t_n)\rangle'_{k'\to 0}\\&=P_{L0}(k')\sum_{i=1}^{n}D_{+i}\left[\frac{1+f_i}{n}+\frac{\partial}{\partial\ln D_{+i}}+(1+f_i)f_i\frac{\partial}{\partial f_i}\right.\\&\left.-(1+f_i)\sum_{j=1}^{n}\left(\delta^K_{i,j}-\frac{1}{n}\right)k_i\frac{\partial}{\partial k_j}\right]\langle\tilde{\delta}^s(k_1,t_1)\ldots\tilde{\delta}^s(k_n,t_n)\rangle'.\end{aligned} \tag{A15}$$

The 3D angular average $\int d\Omega_{\boldsymbol{k}'}/(4\pi)$ of Eq. (37) is replaced by the 1D average $\frac{1}{2}\sum_{\pm k'}$ over the two directions of k' (i.e.,

the two signs of k'). We again defined the reduced polyspectra as in Eq. (38), $\langle\tilde{\delta}^s(k_1)\ldots\tilde{\delta}^s(k_n)\rangle = \langle\tilde{\delta}^s(k_1)\ldots\tilde{\delta}^s(k_n)\rangle'\times\delta_D(k_1+\ldots+k_n)$.

On large scales, we recover the linear theory, with $\tilde{\delta}^s(k',t') \simeq D_+(t')(1+f')\tilde{\delta}_{L0}(k')$, and Eq. (A15) is also written as

$$\frac{1}{2}\sum_{\pm k'}\left\langle\frac{\tilde{\delta}^s(k',t')}{1+f'}\tilde{\delta}^s(k_1,t_1)\ldots\tilde{\delta}^s(k_n,t_n)\right\rangle'_{k'\to 0} = P_L(k',t')\sum_{i=1}^{n}\frac{D_{+i}}{D'_+}\left[\frac{1+f_i}{n}+\frac{\partial}{\partial\ln D_{+i}}+(1+f_i)f_i\frac{\partial}{\partial f_i} - (1+f_i)\sum_{j=1}^{n}\left(\delta^K_{i,j}-\frac{1}{n}\right)k_i\frac{\partial}{\partial k_j}\right]\langle\tilde{\delta}^s(k_1,t_1)\ldots\tilde{\delta}^s(k_n,t_n)\rangle'. \tag{A16}$$

When all times are equal, $t' = t_1 = \ldots = t_n \equiv t$, this simplifies as Eq. (72).

4. Zel'dovich solution

In the 1D case, the Zel'dovich approximation is exact until shell crossing [26,43]. It corresponds to taking for the particle trajectories the linear prediction

$$x(q,t) = q + \Psi_L(q,t) \tag{A17}$$

with

$$\Psi_L(q) = \mathrm{i}\int_{-\infty}^{+\infty}\frac{\mathrm{d}k}{k}e^{\mathrm{i}kq}\tilde{\delta}_L(k,t). \tag{A18}$$

Therefore, the redshift-space coordinate (69) is written as (using $v = a\dot{x}$)

$$s = q + (1+f)\Psi_L \tag{A19}$$

and the redshift-space nonlinear density contrast (70) as Eq. (73).

5. Check of the 1D consistency relations

a. Impact of a large-scale perturbation on the nonlinear redshift-space density contrast

To check the validity of the 1D consistency relations from the exact solution (73), we simply need the change of the nonlinear redshift-space density contrast $\tilde{\delta}^s(k)$ when we make a small perturbation $\Delta\delta_{L0}$ to the initial conditions on much larger scales. Let us consider the impact of a small large-scale perturbation $\Delta\delta_{L0}$ to the initial conditions. Here, we also restrict to even perturbations, $\Delta\tilde{\delta}_{L0}(-k') = \Delta\tilde{\delta}_{L0}(k')$, as the consistency relations studied in this paper apply to spherically averaged statistics, which correspond to the $\pm k'$ averages in the 1D relations (A15)–(A16). Then, expanding Eq. (73) up to first order over $\Delta\delta_{L0}$, and over powers of k', we obtain

$$k'\to 0\colon\ \Delta\tilde{\delta}^s(k) = (1+f)D_+\left[\int\mathrm{d}k'\Delta\tilde{\delta}_{L0}(k')\right]\times\int\frac{\mathrm{d}q}{2\pi}e^{-\mathrm{i}kq+k(1+f)D_+\int\frac{\mathrm{d}k''}{k''}e^{\mathrm{i}k''q}\tilde{\delta}_{L0}(k'')}(\mathrm{i}kq). \tag{A20}$$

Here, the limit $k'\to 0$ means that we consider a perturbation of the initial conditions $\Delta\tilde{\delta}_{L0}(k')$ that is restricted to low wave numbers, $k' < \Lambda$, with a cutoff Λ that goes to zero (i.e., that is much smaller than the wave numbers k and $2\pi/q$ of interest).

On the other hand, from the expression (73), we obtain at once the exact result

$$\frac{\partial\tilde{\delta}^s}{\partial\ln D_+}+(1+f)f\frac{\partial\tilde{\delta}^s}{\partial f}-(1+f)k\frac{\partial\tilde{\delta}^s}{\partial k} = \int\frac{\mathrm{d}q}{2\pi}e^{-\mathrm{i}kq}e^{k(1+f)D_+\int\frac{\mathrm{d}k''}{k''}e^{\mathrm{i}k''q}\tilde{\delta}_{L0}(k'')}(1+f)(\mathrm{i}kq). \tag{A21}$$

The comparison with Eq. (A20) gives

$$k'\to 0\colon\ \Delta\tilde{\delta}^s(k) = D_+\left[\int\mathrm{d}k'\Delta\tilde{\delta}_{L0}(k')\right]\left(\frac{\partial\tilde{\delta}^s(k)}{\partial\ln D_+}+(1+f)f\frac{\partial\tilde{\delta}^s(k)}{\partial f}-(1+f)k\frac{\partial\tilde{\delta}^s(k)}{\partial k}\right). \tag{A22}$$

The consistency relations (A15)–(A16) and (72) only rely on the expression (71), which also reads (at linear order over ϵ_0) as

$$\Delta\tilde{\delta}^s(k) = \epsilon_0 D_+\left(\frac{\partial\tilde{\delta}^s(k)}{\partial\ln D_+}+(1+f)f\frac{\partial\tilde{\delta}^s(k)}{\partial f}-(1+f)k\frac{\partial\tilde{\delta}^s(k)}{\partial k}\right). \tag{A23}$$

Since we have $\epsilon_0 = \Delta\delta_{L0} = \int\mathrm{d}k'\Delta\tilde{\delta}_{L0}(k')$, we recover Eq. (A22). This provides an explicit check of Eq. (71), and hence of the 1D consistency relations.

b. Explicit check on the redshift-space density polyspectra

Instead of looking for the impact of a large-scale linear perturbation on the nonlinear density contrast, as in Sec. A 5 a, we can directly check the consistency relations in their form (A15) or (72). Considering for simplicity the equal-time polyspectra (72), we define the mixed

polyspectra, formed by one linear density contrast and n nonlinear redshift-space density contrasts,

$$E_n^s(k';k_1,\ldots,k_n;t) \equiv \langle \tilde{\delta}_L(k',t)\tilde{\delta}^s(k_1,t)\ldots\tilde{\delta}^s(k_n,t)\rangle = D_+\left\langle \tilde{\delta}_{L0}(k')\int\frac{\mathrm{d}q_1\ldots\mathrm{d}q_n}{(2\pi)^n}e^{-\mathrm{i}\sum_{j=1}^n k_jq_j} \times e^{(1+f)D_+\int \mathrm{d}k/k\tilde{\delta}_{L0}(k)\sum_{j=1}^n k_je^{\mathrm{i}kq_j}}\right\rangle, \tag{A24}$$

where in the last expression we used Eq. (73). The Gaussian average over the initial conditions $\tilde{\delta}_{L0}$ gives

$$E_n^s = -\frac{P_L(k')}{k'}(1+f)\int\frac{\mathrm{d}q_1\ldots\mathrm{d}q_n}{(2\pi)^n}\sum_{j=1}^n k_je^{-\mathrm{i}k'q_j} \times e^{-\mathrm{i}\sum_{j=1}^n k_jq_j-(1+f)^2D_+^2/2\int \mathrm{d}k/k^2P_{L0}(k)|\sum_{j=1}^n k_je^{\mathrm{i}kq_j}|^2}. \tag{A25}$$

Making the changes of variable $q_1 = q_1' + q_n, \ldots, q_{n-1} = q_{n-1}' + q_n$, the argument of the last exponential does not depend on q_n. Then, the integration over q_n yields a Dirac factor $\delta_D(k' + k_1 + \ldots + k_n)$, that we factor out by defining $E_n^s = E_n^{s'}\delta_D(k' + k_1 + \ldots + k_n)$, with a primed notation as in Eq. (38), and we replace k_n by $-(k' + k_1 + \ldots + k_{n-1})$. Finally, in the limit $k' \to 0$, we expand the terms $e^{-\mathrm{i}k'q_j}$ up to first order over k', and we obtain

$$k' \to 0\colon\ E_n^{s'} = P_L(k')(1+f)\int\frac{\mathrm{d}q_1\ldots\mathrm{d}q_{n-1}}{(2\pi)^{n-1}} \times\left[1+\mathrm{i}\sum_{j=1}^{n-1}k_jq_j\right]e^{-\mathrm{i}\sum_{j=1}^{n-1}k_jq_j} \times e^{-(1+f)^2D_+^2/2\int \mathrm{d}k/k^2P_{L0}(k)|\sum_{j=1}^{n-1}k_j(e^{\mathrm{i}kq_j}-1)|^2}. \tag{A26}$$

Proceeding in the same fashion, the n-point redshift-space polyspectra read as

$$P_n^s \equiv \langle\tilde{\delta}^s(k_1,t)\ldots\tilde{\delta}^s(k_n,t)\rangle' = \int\frac{\mathrm{d}q_1\ldots\mathrm{d}q_{n-1}}{(2\pi)^{n-1}}e^{-\mathrm{i}\sum_{j=1}^{n-1}k_jq_j} \times e^{-(1+f)^2D_+^2/2\int \mathrm{d}k/k^2P_{L0}(k)|\sum_{j=1}^{n-1}k_j(e^{\mathrm{i}kq_j}-1)|^2}. \tag{A27}$$

Then, we can explicitly check from the comparison with Eq. (A26) that we have the relation

$$k' \to 0\colon\ E_n^{s'} = P_L(k')\left[1+f+\frac{\partial}{\partial\ln D_+}+(1+f)f\frac{\partial}{\partial f} - (1+f)\sum_{i=1}^{n-1}\frac{\partial}{\partial\ln k_i}\right]P_n^s, \tag{A28}$$

and we recover the consistency relation (72). [In Eq. (A28), the right-hand side does not involve k_n because it has been replaced by $-(k_1 + \ldots + k_{n-1})$ in Eq. (A27), using the Dirac factor $\delta_D(k_1 + \ldots + k_n)$.]

[1] A. Albrecht *et al.*, arXiv:astro-ph/0609591.
[2] R. Laureijs *et al.*, arXiv:1110.3193.
[3] M. H. Goroff, B. Grinstein, S.-J. Rey, and M. B. Wise, Astrophys. J. **311**, 6 (1986).
[4] F. Bernardeau, S. Colombi, E. Gaztañaga, and R. Scoccimarro, Phys. Rep. **367**, 1 (2002).
[5] M. Crocce and R. Scoccimarro, Phys. Rev. D **73**, 063519 (2006).
[6] P. Valageas, Astron. Astrophys. **465**, 725 (2007).
[7] M. Pietroni, J. Cosmol. Astropart. Phys. 10 (2008) 036.
[8] F. Bernardeau, M. Crocce, and R. Scoccimarro, Phys. Rev. D **78**, 103521 (2008).
[9] A. Taruya, F. Bernardeau, T. Nishimichi, and S. Codis, Phys. Rev. D **86**, 103528 (2012).
[10] M. Crocce, R. Scoccimarro, and F. Bernardeau, Mon. Not. R. Astron. Soc. **427**, 2537 (2012).
[11] F. Bernardeau, N. Van de Rijt, and F. Vernizzi, Phys. Rev. D **87**, 043530 (2013).
[12] P. Valageas, T. Nishimichi, and A. Taruya, Phys. Rev. D **87**, 083522 (2013).
[13] M. Pietroni, G. Mangano, N. Saviano, and M. Viel, J. Cosmol. Astropart. Phys. 01 (2012) 019.
[14] D. Baumann, A. Nicolis, L. Senatore, and M. Zaldarriaga, J. Cosmol. Astropart. Phys. 07 (2012) 051.
[15] J. J. M. Carrasco, S. Foreman, D. Green, and L. Senatore, J. Cosmol. Astropart. Phys. 07 (2014) 057.
[16] T. Baldauf, L. Mercolli, M. Mirbabayi, and E. Pajer, J. Cosmol. Astropart. Phys. 05 (2015) 007.
[17] A. Kehagias and A. Riotto, Nucl. Phys. **B873**, 514 (2013).
[18] M. Peloso and M. Pietroni, J. Cosmol. Astropart. Phys. 05 (2013) 031.
[19] P. Creminelli, J. Noreña, M. Simonović, and F. Vernizzi, J. Cosmol. Astropart. Phys. 12 (2013) 025.
[20] A. Kehagias, J. Noreña, H. Perrier, and A. Riotto, Nucl. Phys. **B883**, 83 (2014).
[21] M. Peloso and M. Pietroni, J. Cosmol. Astropart. Phys. 04 (2014) 011.

[22] P. Creminelli, J. Gleyzes, M. Simonović, and F. Vernizzi, J. Cosmol. Astropart. Phys. 02 (2014) 051.
[23] P. Valageas, Phys. Rev. D **89**, 083534 (2014).
[24] P. Creminelli, J. Gleyzes, L. Hui, M. Simonović, and F. Vernizzi, J. Cosmol. Astropart. Phys. 06 (2014) 009.
[25] A. Kehagias, A. Moradinezhad Dizgah, J. Noreña, H. Perrier, and A. Riotto, J. Cosmol. Astropart. Phys. 08 (2015) 018.
[26] P. Valageas, Phys. Rev. D **89**, 123522 (2014).
[27] A. Kehagias, H. Perrier, and A. Riotto, Mod. Phys. Lett. A **29**, 1450152 (2014).
[28] T. Nishimichi and P. Valageas, Phys. Rev. D **90**, 023546 (2014).
[29] C.-T. Chiang, C. Wagner, F. Schmidt, and E. Komatsu, J. Cosmol. Astropart. Phys. 05 (2014) 048.
[30] I. Ben-Dayan, T. Konstandin, R. A. Porto, and L. Sagunski, J. Cosmol. Astropart. Phys. 02 (2015) 026.
[31] C. Wagner, F. Schmidt, C.-T. Chiang, and E. Komatsu, J. Cosmol. Astropart. Phys. 08 (2015) 042.
[32] R. Scoccimarro, H. M. P. Couchman, and J. A. Frieman, Astrophys. J. **517**, 531 (1999).
[33] R. Scoccimarro, Phys. Rev. D **70**, 083007 (2004).
[34] J. C. Jackson, Mon. Not. R. Astron. Soc. **156**, 1P (1972).
[35] N. Kaiser, Mon. Not. R. Astron. Soc. **227**, 1 (1987).
[36] A. N. Taylor and A. J. S. Hamilton, Mon. Not. R. Astron. Soc. **282**, 767 (1996).
[37] P. Valageas, Astron. Astrophys. **526**, A67 (2011).
[38] P. J. E. Peebles, *The Large-Scale Structure of the Universe* (Princeton University, Princeton, NJ, 1980).
[39] M. Crocce, S. Pueblas, and R. Scoccimarro, Mon. Not. R. Astron. Soc. **373**, 369 (2006).
[40] P. Valageas, Astron. Astrophys. **484**, 79 (2008).
[41] T. Baldauf, U. Seljak, L. Senatore, and M. Zaldarriaga, J. Cosmol. Astropart. Phys. 10 (2011) 031.
[42] F. R. Bouchet, R. Juszkiewicz, S. Colombi, and R. Pellat, Astrophys. J. Lett. **394**, L5 (1992).
[43] Y. B. Zel'Dovich, Astron. Astrophys. **5**, 84 (1970).
[44] V. Springel, Mon. Not. R. Astron. Soc. **364**, 1105 (2005).
[45] R. Scoccimarro, Mon. Not. R. Astron. Soc. **299**, 1097 (1998).
[46] T. Nishimichi *et al.*, Publ. Astron. Soc. Jpn. **61**, 321 (2009).
[47] E. Komatsu *et al.*, Astrophys. J. Suppl. Ser. **148**, 119 (2003).
[48] A. Taruya, T. Nishimichi, and S. Saito, Phys. Rev. D **82**, 063522 (2010).
[49] T. Matsubara, Phys. Rev. D **77**, 063530 (2008).
[50] U. Seljak and P. McDonald, J. Cosmol. Astropart. Phys. 11 (2011) 039.
[51] E. Jennings, C. M. Baugh, and S. Pascoli, Mon. Not. R. Astron. Soc. **410**, 2081 (2011).
[52] B. A. Reid and M. White, Mon. Not. R. Astron. Soc. **417**, 1913 (2011).